
Federated Concept-Based Models: Interpretable models with distributed supervision

Dario Fenoglio ^{*1} Arianna Casanova ^{*2} Francesco De Santis³ Mohan Li¹ Gabriele Dominici¹
 Johannes Schneider² Martin Gjoreski¹ Marc Langheinrich¹ Pietro Barbiero⁴ Giovanni De Felice¹

Abstract

Concept-based models (CMs) enhance interpretability in deep learning by grounding predictions in human-understandable concepts. However, concept annotations are expensive to obtain and rarely available at scale within a single data source. Federated learning (FL) could alleviate this limitation by enabling cross-institutional training that leverages concept annotations distributed across multiple data owners. Yet, FL lacks interpretable modeling paradigms. Integrating CMs with FL is non-trivial: CMs assume a fixed concept space and a predefined model architecture, whereas real-world FL is heterogeneous and non-stationary, with institutions joining over time and bringing new supervision. In this work, we propose *Federated Concept-based Models* (F-CMs), a new methodology for deploying CMs in evolving FL settings. F-CMs aggregate concept-level information across institutions and efficiently adapt the model architecture in response to changes in the available concept supervision, while preserving institutional privacy. Empirically, F-CMs preserve the accuracy and intervention effectiveness of training settings with full concept supervision, while outperforming non-adaptive federated baselines. Notably, F-CMs enable interpretable inference on concepts not available to a given institution, a key novelty with respect to existing approaches.

1. Introduction

In many real-world applications, the deployment of machine learning systems is subject to constraints beyond predictive accuracy: practitioners need models whose predictions are interpretable and auditable, providing tools for error diagnosis, fairness assessment, and compliance with legal standards (Kaminski, 2021; Li et al., 2022; Dhar et al., 2023). Among existing approaches, *concept-based models* (CMs) offer an established framework in which predictions are formulated in terms of high-level, human-interpretable variables, referred to as *concepts* (Koh et al., 2020; Espinosa Zarlenaga et al., 2022). In practice, however, their applicability is constrained by the need for explicit concept supervision during training (Debole et al., 2025; Poeta et al., 2023). Concept annotations are costly, time-consuming, and rarely available at scale within a single data source.

A natural way to alleviate this limitation is to pool concept knowledge across multiple data owners, such as hospitals, research centers, or devices (Litjens et al., 2018; Kaassis et al., 2020). Federated learning (FL) provides a principled paradigm for collaborative training without sharing raw data, making it particularly appealing in privacy-sensitive settings where concept annotations themselves may encode sensitive information (McMahan et al., 2023). Yet, current FL frameworks lack modeling paradigms that support concept-level interpretability. Existing CM formulations are poorly aligned with realistic federated deployments because they typically assume a fixed concept space and a concept-dependent architecture designed upfront. In contrast, real-world FL systems are inherently *evolving*, i.e., participating institutions (*clients*) may rely on heterogeneous annotations, and can join or leave over time, requiring updates not only to learned parameters but also to the model structure itself (Jothimurugesan et al., 2023; Jarczewski et al., 2024; Fenoglio et al., 2025; Li et al., 2026).

To bridge this gap, we introduce *Federated Concept-based Models* (F-CMs), a new methodology for deploying concept-based architectures in evolving federated settings. Crucially, F-CMs handle *statistical heterogeneity* and *temporal non-stationarity*: as new clients join (potentially from new data distributions), they may introduce previously unseen con-

^{*}Equal contribution ¹Università della Svizzera italiana, Lugano, Switzerland ²University of Liechtenstein, Vaduz, Liechtenstein ³Politecnico di Torino, Turin, Italy ⁴IBM Research, Zurich, Switzerland. Correspondence to: Dario Fenoglio <dario.fenoglio@usi.ch>, Arianna Casanova <arianna.casanova@uni.li>.

cepts and novel dependencies. To accommodate this, F-CMs expand the shared concept space and, when available, update the concept dependency structure, while adapting the architecture modularly—updating only the affected components—thereby avoiding full retraining and preserving previously learned knowledge. To the best of our knowledge, F-CMs are the first to address evolving concept spaces under temporal non-stationarity (dynamic participation and data drift) via structure-aware modular architecture adaptation, rather than a fixed model.

Our methodology benefits both communities. On the one hand, it provides a systematic way to incorporate concept-based interpretability into evolving FL settings; on the other hand, within concept-based modeling, it reduces the need for concept annotations at a single institution by enabling privacy-preserving knowledge sharing. Our key contributions are:

- We introduce **F-CMs, a new methodology for deploying concept-based architectures in realistic federated settings**, addressing heterogeneous, partial concept supervision and temporal non-stationarity.
- We instantiate F-CMs with four CM architectures and validate them on five synthetic benchmarks and a real-life medical imaging dataset, demonstrating **strong predictive and intervention performance, interpretable inference for concepts unannotated** at a given institution, and **reduced retraining cost** under federation growth.

2. Preliminaries

In this section we introduce key preliminaries on concept-based models (CMs) and federated learning (FL).

2.1. Concept-based models (CMs)

Bipartite CMs (Koh et al., 2020; Espinosa Zarlenga et al., 2022). Decompose prediction in two stages: (i) mapping inputs to human-interpretable *concepts*, and (ii) predicting the downstream task from these concepts. Formally, let \mathcal{X} denote the input space and \mathcal{Y} the output space. A bipartite CM consists of: (i) a *concept encoder* $h : \mathcal{X} \rightarrow \mathcal{C}$ that maps an input $x \in \mathcal{X}$, or a learned latent representation thereof, to a set of m predicted concepts $\hat{c} = (\hat{c}_1, \dots, \hat{c}_m)$, where each \hat{c}_j may be a scalar or a vector; and (ii) a *task decoder* $f : \mathcal{C} \rightarrow \mathcal{Y}$ that maps predicted concepts to a task prediction \hat{y} . The overall prediction is given by $\hat{y} = f(h(x))$. In practice, h and f are instantiated as parametric functions (e.g., neural networks).

The task decoder can be interpreted as operating on a *directed acyclic graph* (DAG) (Pearl, 1995), $\mathcal{G} = (\mathcal{V}, \mathcal{E})$, with nodes $\mathcal{V} = \{C_1, \dots, C_m, Y\}$, where each $C_j \in \mathcal{V}$ represents a concept and $Y \in \mathcal{V}$ the task. Edges exist only from

C_j to the task Y , reflecting the assumption that concepts predictions are conditionally independent given the input.

Graph-Based CMs (Dominici et al., 2024; De Felice et al., 2025). Extend bipartite CMs by allowing structured dependencies among concepts (and tasks), represented through a more general DAG \mathcal{G} , which also includes edges between concepts. Bipartite CMs arise as a special case, when \mathcal{E} contains only directed edges from concepts to the task. In graph-based CMs, each concept prediction is computed as a function of its parent nodes in the graph and an additional input-dependent factor (interpreted as a latent factor in the graph): $\hat{c}_j = h_j(\hat{c}_{\text{PA}(C_j)}, u_j)$, where $\text{PA}(C_j)$ denotes the parents of C_j in \mathcal{G} , h_j is a learnable (parametric) function, and u_j captures information extracted from the input x that is not explained by parent concepts, needed to predict C_j . The task prediction follows analogously as $\hat{y} = f(\hat{c}_{\text{PA}(Y)}, u_Y)$, where f is a learnable (parametric) function. Notably, graph-based CMs yield more interpretable concept predictions by making explicit which other concepts each concept depends on.

2.2. Federated Learning (FL)

FL trains a shared model across multiple data owners (*clients*) without sharing raw data (McMahan et al., 2023). In general, the client population may be time-varying, denoted as $\mathcal{K}(t)$; at round t , the server selects a participating subset $\mathcal{K}_t \subseteq \mathcal{K}(t)$ (partial participation) (Jarczewski et al., 2024; De Oliveira Jarczewski et al., 2025). Each client $k \in \mathcal{K}(t)$ holds a private dataset $\mathcal{D}^{(k)} = \{(x_i^{(k)}, y_i^{(k)})\}_{i=1}^{n^{(k)}}$ with $x_i^{(k)} \in \mathcal{X}$ and $y_i^{(k)} \in \mathcal{Y}$. Let $m_{\mathbf{w}} : \mathcal{X} \rightarrow \mathcal{Y}$ be a parametric model with parameters \mathbf{w} and loss $\ell(\cdot, \cdot)$. FL minimizes a weighted global objective

$$\min_{\mathbf{w}} \sum_{k=1}^K p_k F_k(\mathbf{w}), \quad F_k(\mathbf{w}) = \mathbb{E}_{(x, y) \sim \mathcal{D}^{(k)}} [\ell(m_{\mathbf{w}}(x), y)],$$

where p_k typically weighs clients proportionally to their data size. At round t , the server broadcasts \mathbf{w}_t to a subset of available clients $k \in \mathcal{K}_t$. Each selected client performs E steps (or epochs) of local optimization (e.g., SGD) on $\mathcal{D}^{(k)}$ to obtain an updated model $\mathbf{w}_{t+1}^{(k)}$, and sends it back to the server. The server then aggregates client updates, e.g., via FedAvg, weighting each client proportionally to its local dataset size $n^{(k)} = |\mathcal{D}^{(k)}|$:

$$\mathbf{w}_{t+1} = \sum_{k \in \mathcal{K}_t} \frac{n^{(k)}}{\sum_{j \in \mathcal{K}_t} n^{(j)}} \mathbf{w}_{t+1}^{(k)}. \quad (1)$$

Statistical heterogeneity and temporal non-stationarity. Practical FL deployments are rarely stationary (Xiang et al., 2024). First, FL is typically *statistically heterogeneous*: different clients observe different data distributions, i.e., $\exists k \neq k' \text{ s.t. } \mathbb{P}_k(X, Y) \neq \mathbb{P}_{k'}(X, Y)$, so their local objec-

tives F_k differ (Kairouz et al., 2021). Second, FL can be *temporally non-stationary*, meaning that the data and/or the set of participating clients changes over rounds. This happens in two common ways: (i) *dynamic client participation*, where the available client pool $\mathcal{K}(t)$ and the sampled participants \mathcal{K}_t vary over time as clients join or leave (De Oliveira Jarzefski et al., 2025); and (ii) *data drift*, where even for a fixed client k , its distribution changes over time, i.e., $\mathbb{P}_k^{(t)}(X, Y) \neq \mathbb{P}_k^{(t')}(X, Y)$ for $t \neq t'$ (Panchal et al., 2023). Both effects induce a time-varying optimization landscape and can destabilize global updates.

These FL conditions violate key assumptions underlying standard CMs, making their integration challenging. Standard CMs assume a fixed concept set and, for graph-based variants, a predefined concept-dependency structure that determines the architecture. In federated deployments, concept annotations are distributed across clients and may evolve as new clients or data become available, so the set of concepts and their dependencies can change over time. Consequently, a federated CM must (i) reconcile heterogeneous, partial concept information across clients, and (ii) dynamically update concept dependencies and corresponding architecture during training, rather than relying on a fixed design.

3. Problem Setting

We study the problem of learning CMs in a federated setting with statistical heterogeneity and temporal non-stationarity (Section 2.2).¹ All clients share an input space \mathcal{X} and a task label space \mathcal{Y} . Training proceeds over rounds $t = 1, \dots, T$, where a subset of clients \mathcal{K}_t participates. Client k holds a local dataset $\mathcal{D}^{(k)} = \{(x_i^{(k)}, c_i^{(k)}, y_i^{(k)})\}_{i=1}^{n^{(k)}}$, where $x_i^{(k)} \in \mathcal{X}$, while concept annotations $c_i^{(k)}$ and task labels $y_i^{(k)}$ may be missing (however we assume each client has at least some concept or task supervision). Let $I^{(k)}$ be the index set of concepts supervised at client k . As participation evolves, so does the shared supervised concept set; we define the federation concept set up to round t as $\mathcal{M}_t := \bigcup_{\tau=1}^t \bigcup_{k \in \mathcal{K}_\tau} I^{(k)}$. Optionally, each client k may provide a local DAG $\mathcal{G}^{(k)}$ over its supervised concepts $I^{(k)}$ (and the task label Y when available), represented as either a binary adjacency matrix $A^{(k)}$ with $A_{ij}^{(k)} = 1$ for an edge $i \rightarrow j$, or an edge-confidence matrix $S^{(k)}$ encoding confidence in each edge.

The goal is to **learn a shared bipartite or graph-based CM while preserving privacy** by restricting communication to model updates (and optional graph-level information).

¹Client-level data drift can be absorbed by viewing a client whose data distribution changes over time as a sequence of “virtual” clients appearing in different rounds; we omit explicit time indices to keep notation light.

4. Method

In this section, we introduce **Federated Concept-based Models (F-CMs)**, a methodology for learning CMs in federated settings with *partial, heterogeneous concept supervision* under *temporal non-stationarity* (Section 3). F-CMs apply to both *bipartite* CMs (Section 2.1) and *graph-based* CMs (Section 2.1). As in standard FL, F-CMs maintain a single shared CM whose parameters are optimized through repeated rounds of client-side training and server-side aggregation. Unlike classical FL, F-CMs handle an evolving concept space and introduce three key extensions: (i) at each round t , the server aggregates client-provided dependency information ($A^{(k)}$ or $S^{(k)}$) into a shared DAG \mathcal{G}_t that may be used to define the model architecture; (ii) the shared architecture is updated efficiently when new concepts or graph dependencies appear, modifying only affected modules; and (iii) supervision is module-specific, i.e., each client updates only the modules corresponding to the variables they have annotations for. Algorithm 1 in Appendix D.2 summarizes the methodology.

4.1. F-CM Shared Model

At each round t , the server maintains a shared CM parameterized by $\mathbf{w}_t = (\theta_t, \phi_t, \psi_t)$. The model follows a standard CM design:

- an *input encoder* $g_{\theta_t} : \mathcal{X} \rightarrow \mathbb{R}^d$ that maps $x \in \mathcal{X}$ to $z = g_{\theta_t}(x)$;
- a collection of *concept encoders* $\{h_{\phi_t, j}\}_{j \in \mathcal{M}_t}$ producing concept predictions $\hat{c}_j = h_{\phi_t, j}(\hat{c}_{B_j(t)}, z) \in \mathcal{C}_j, j \in \mathcal{M}_t$, where $B_j(t) \subseteq \mathcal{M}_t \setminus \{j\}$ is an (possibly empty) index set that specifies which other concept predictions are provided as inputs to the j -th module at round t , and $\hat{c}_{B_j(t)} = \{\hat{c}_\ell\}_{\ell \in B_j(t)}$;
- a *task decoder* f_{ψ_t} producing $\hat{y} = f_{\psi_t}(\hat{c}_{B_Y(t)}, z) \in \mathcal{Y}$, for some index set $B_Y(t) \subseteq \mathcal{M}_t$.

\mathcal{M}_t , $\{B_j(t)\}_{j \in \mathcal{M}_t}$, and $B_Y(t)$ determine the model connectivity at round t : for each concept j , $B_j(t)$ lists the concept predictions used to compute \hat{c}_j , and $B_Y(t)$ lists those used to compute \hat{y} . Both may change over time (see Section 4.2.2). The specific functional forms of $\{h_{\phi_t, j}\}$ and f_{ψ_t} depend on the chosen CM instantiation (Section 4.3).

4.2. F-CM Training Pipeline

At each round t , F-CM sequentially: (i) **aggregates available client-proposed DAG $\mathcal{G}^{(k)}$** (Sec. 4.2.1); (ii) **adapts the shared architecture** (Sec. 4.2.2); (iii) **performs module-specific training and module-wise aggregation** (Sec. 4.2.3); Fig. 1 provides an overview.

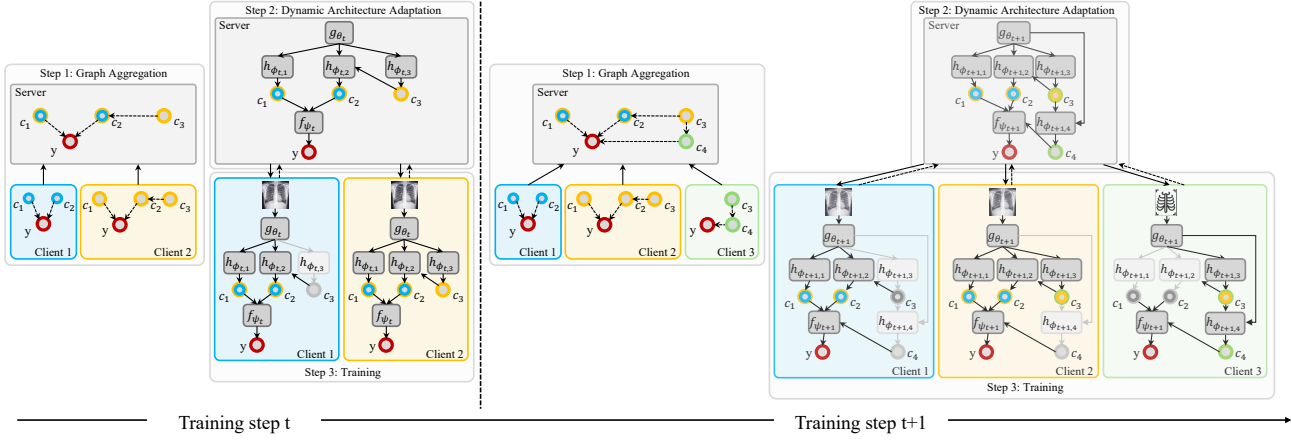


Figure 1. F-CMs overview. At each round t , F-CMs performs three steps. (1) *Graph aggregation*: the server combines the concept graphs provided by participating clients into a shared graph \mathcal{G}_t . (2) *Architecture update*: the shared CM is updated to reflect \mathcal{G}_t and/or the concepts known at round t (only newly introduced or rewired modules are changed). (3) *Training*: the server broadcasts the model; each client trains only modules for concepts (and task) it supervises (dark grey), leaving the others frozen (light grey), and the server aggregates the corresponding module updates. The figure shows two consecutive rounds, where newly arriving clients introduce new concepts.

4.2.1. GRAPH AGGREGATION

In federated deployments, a single client’s structural knowledge can be unreliable: local graphs may be noisy due to limited, non-IID data, and (in open or cross-silo settings) can be manipulated by compromised clients (i.e., poisoning) (Sun et al., 2022). We therefore aggregate client-provided structure into a shared graph by favoring edges and directions with the strongest support across participants. Each client $k \in \mathcal{K}_t$ may send to the server a binary adjacency matrix $A^{(k)}$ or an edge-confidence matrix $S^{(k)}$ defined over the concepts they supervise. **The server aggregates the information to estimate a shared graph, keeping edges and directions receiving the strongest support.**

Specifically, we interpret $S_{ij}^{(k)}$ as the client’s probability for the directed edge $i \rightarrow j$. Hence, for each unordered pair $\{i, j\}$ with $i \neq j$, we can define a three-way distribution over $\{i \rightarrow j, j \rightarrow i, \emptyset\}$ by setting $S^{(k)}(\emptyset)_{ij} := 1 - S_{ij}^{(k)} - S_{ji}^{(k)}$, where $S^{(k)}(\emptyset)_{ij}$ denotes the probability that there is no edge between i and j . When confidence scores are not available, we set $S^{(k)} \equiv A^{(k)}$. The server aggregates client scores into a *strength* matrix by summing contributions from clients that observe both nodes:

$$[\bar{S}_t]_{ij} := \sum_{k \in \mathcal{K}_t: i, j \in I^{(k)}} \alpha_k S_{ij}^{(k)},$$

where α_k are aggregation weights (e.g., proportional to client dataset sizes), and $[\bar{S}_t]_{ij} = 0$ if the sum is empty. Analogous calculations are performed to obtain $\bar{S}_t(\emptyset)_{ij}$. We then decide edge existence and orientation taking the maximum over the three outcomes:

$$(i \rightarrow j) \in \tilde{\mathcal{G}}_t \iff [\bar{S}_t]_{ij} = \max\{[\bar{S}_t]_{ij}, [\bar{S}_t]_{ji}, \bar{S}_t(\emptyset)_{ij}\},$$

If the maximum is attained by multiple options, one is chosen randomly. The resulting candidate graph $\tilde{\mathcal{G}}_t$ is finally

projected to a DAG \mathcal{G}_t by iteratively resolving cycles.

4.2.2. DYNAMIC ARCHITECTURE ADAPTATION

Under non-stationarity, new clients may introduce previously unseen concepts or revise existing dependencies. In particular, we assume a monotone federation: when clients leave, the server retains the concepts and dependency information accumulated so far. Accordingly, F-CMs adapt the shared CM by updating the architecture only when module interfaces change, while preserving all unaffected modules. At round t **the server updates the model to match the current concept set \mathcal{M}_t and, in graph-based instantiations, the aggregated graph \mathcal{G}_t .** The encoder g_{θ_t} is unchanged; only $\{h_{\phi_t, j}\}_j$ and f_{ψ_t} may be modified.²

(E1) Adding a new concept. For any newly observed concept j , the server instantiates a new module $h_{\phi_t, j}$. The task decoder is expanded to accept the new concept input if $j \in B_Y(t)$, while all other modules are left unchanged.

(E2) Updating an edge (add/remove/re-orient). When \mathcal{G}_t is used (i.e., in graph-based instantiations), any change in the relation between two nodes i and j may alter the parent set of one (or both) nodes and therefore the input sets of the affected modules. Concretely, adding $i \rightarrow j$ appends \hat{c}_i to the inputs of $h_{\phi, j}$; removing $i \rightarrow j$ drops that input. Re-orienting an edge $i \rightarrow j$ into $j \rightarrow i$ is treated as a remove+add operation, updating both modules: $h_{\phi, j}$ loses \hat{c}_i as input, while $h_{\phi, i}$ gains \hat{c}_j . The task module is updated analogously whenever B_Y changes due to an update in \mathcal{G}_t . In bipartite instantiations edge updates do not affect the architecture.

²In graph-based F-CM instantiations, we assume a shared graph \mathcal{G}_t is available for concepts in the federation. Concepts not present in the graph are ignored.

Warm-start initialization. Whenever a module input interface is expanded, newly introduced parameters are initialized while preserving the existing ones (e.g., zero-initializing the weights connected to new inputs to keep the pre-update behavior at initialization, or standard random initialization). Modules whose interfaces are unchanged retain their parameters exactly, avoiding full retraining.

4.2.3. MODULE-SPECIFIC TRAINING AND MODULE-WISE AGGREGATION

Because concept and task supervision are unevenly distributed across clients, vanilla FedAvg would mix updates for modules that some clients cannot supervise. F-CMs thus perform module-specific training and module-wise aggregation, restricting contributions to supervised components.

Module-specific local optimization. At round t , each client $k \in \mathcal{K}_t$ receives the current global state $(\tilde{\mathbf{w}}_t, \mathcal{G}_t)$, with \mathcal{G}_t provided only when available, and performs E local optimization steps using only the supervision available at k . The local objective is

$$\mathcal{L}^{(k)}(\tilde{\mathbf{w}}_t; \mathcal{G}_t) = \gamma \sum_{j \in I^{(k)}} \mathcal{L}_c(\hat{c}_j^{(k)}, c_j^{(k)}) + (1 - \gamma) \mathbf{1}_{\{k \in \mathcal{K}_t^{(Y)}\}} \mathcal{L}_t(\hat{y}^{(k)}, y^{(k)}), \quad (2)$$

where \mathcal{L}_c and \mathcal{L}_t are standard losses for concepts and task (e.g., cross-entropy or MSE depending on variable type), $\mathcal{K}_t^{(Y)}$ are clients in \mathcal{K}_t who supervise Y , and $\gamma \in [0, 1]$. Only supervised concept encoders $j \in I^{(k)}$ and/or task decoder contribute gradients. Modules without supervision are frozen, ensuring that each client updates only the components it can supervise.

Module-wise aggregation. The server aggregates each module using only the clients that produced updates for that module. Let $\mathcal{U}_t^j \subseteq \mathcal{K}_t$ denote the clients updating concept module $h_{\phi_{t,j}}$, yielding local parameters $\phi_{t+1,j}^{(k)}$. The aggregated parameters are

$$\phi_{t+1,j} = \sum_{k \in \mathcal{U}_t^j} \beta_j^{(k)} \phi_{t+1,j}^{(k)}, \quad \beta_j^{(k)} = \frac{n^{(k)}}{\sum_{r \in \mathcal{U}_t^j} n^{(r)}}.$$

The task module is aggregated analogously over clients that updated it, while modules not updated by any client remain unchanged. The encoder parameters are aggregated using standard FedAvg over the participating clients.

4.3. Instantiations

F-CMs are agnostic to the specific CM architecture used as the shared model. An instantiation specifies the parameterization of modules $\{h_{\phi_{t,j}}\}_j$ and f_{ψ_t} . In this work, we instantiate F-CMs with two bipartite families and two graph-based families, described next (additional details in Appendix D).

Bipartite instantiations. (i) **Concept Bottleneck Models (CBMs)** (Koh et al., 2020), where each $h_{\phi_{t,j}}$ outputs a scalar concept prediction and f_{ψ_t} composes these predictions to produce \hat{y} ; (ii) **Concept Embedding Models (CEMs)** (Espinosa Zarlenga et al., 2022), where, differently from CBMs, each $h_{\phi_{t,j}}$ outputs an embedding for each concept. The task decoder operates analogously to produce \hat{y} .

Graph-based instantiations. (i) **Causal Concept Graph Models (CGMs)** (Dominici et al., 2024), where each concept encoder $h_{\phi_{t,j}}$ predicts a concept by conditioning on its parents (and the input representation), so that predictions are propagated along the graph; the task decoder is treated analogously as the predictor for the node Y , depending only on its parents. (ii) **Causally Reliable CBMs (C²BMs)** (De Felice et al., 2025), which use the same DAG-based factorization but additionally equip each node with a node-specific input-dependent signal that is combined with the parent-based mechanism.

5. Experimental Evaluation

We empirically evaluate F-CMs across both interpretability and FL objectives. Specifically, we assess (i) task accuracy and concept coverage (Section 5.1), (ii) accuracy under ground-truth interventions (Section 5.2), (iii) training efficiency under evolving federations with dynamic architecture adaptation (Section 5.3), and (iv) privacy–utility trade-offs under client-level differential privacy (Appendix E.4). Additional sensitivity analyses (number of clients, selective parameter freezing) are reported in Appendix E.5, and robustness to noisy client graphs is reported in Appendix E.6.

Baselines and training regimes. We compare F-CMs instantiations to an opaque neural baseline (**OpaqNN**) under four training regimes: (i) **Centralized (Cent.)**, pooling all client data and available concept annotations; (ii) **F-CMs** (ours); (iii) **S-F-CMs**, a static federated baseline to enable comparison in federated settings, which follows the same optimization and structure aggregation as F-CMs, but fixes the concept space and architecture after the first-round client participation (no adaptation); (iv) **Localized (Loc.)**, training independent models per client without sharing.

Federated protocol under temporal non-stationarity. Federated experiments are conducted under *non-stationarity* driven by dynamic participation. At each round t , the server samples $|\mathcal{K}_t| = 10$ clients. The client pool $\mathcal{K}(t)$ evolves during training, reaching a total of 20 clients: after an initial warm-up phase (at $t = 10$ for ASIA, SACHS, and SIIM, and at $t = 20$ otherwise; Appendix D.1), new clients join, introducing new concept supervision and, for graph-based instantiations, potentially novel dependencies. Additional experiments scaling up to $|\mathcal{K}_t| = 100$ are in Appendix E.5.1.

Datasets and data preparation. We consider five

Table 1. Task accuracy (%) and concept coverage (%) with respect to the ground-truth concepts causally relevant for the task. Methods that improve the average performance are shown in bold.

Setting	Method	Asia		Sachs		Alarm		Insurance		Hailfinder		SIIM-Pn.	
		T	C. Cov.	T	C. Cov.	T	C. Cov.	T	C. Cov.	T	C. Cov.	T	C. Cov.
Cent. (Upper Bound)	OpaqNN	80.6 \pm 2.0	100	77.5 \pm 2.1	100	73.6 \pm 1.5	100	76.6 \pm 2.0	100	73.2 \pm 0.8	100	75.5 \pm 0.8	100
	CBM	79.9 \pm 2.0	100	77.2 \pm 1.7	100	73.7 \pm 1.2	100	76.4 \pm 2.0	100	75.8 \pm 1.5	100	75.1 \pm 0.6	100
	CEM	80.6 \pm 2.0	100	77.6 \pm 1.7	100	70.7 \pm 0.6	100	76.2 \pm 2.2	100	72.6 \pm 1.9	100	75.1 \pm 0.4	100
	CGM	79.3 \pm 2.2	100	76.5 \pm 1.7	100	70.4 \pm 1.2	100	73.2 \pm 1.9	100	72.4 \pm 1.8	100	69.5 \pm 2.2	100
	C ² BM	80.1 \pm 2.0	100	77.4 \pm 1.8	100	72.0 \pm 1.2	100	75.1 \pm 2.0	100	74.1 \pm 1.8	100	74.4 \pm 0.6	100
Loc.	OpaqNN	62.9 \pm 8.8	43.3 \pm 4.1	55.1 \pm 16.1	56 \pm 4.0	36.1 \pm 18.2	40.9 \pm 7.1	19.2 \pm 12.3	70.5 \pm 7.4	44.7 \pm 15.2	63.7 \pm 3.5	61.5 \pm 4.7	37.5 \pm 0.4
	CBM	48.7 \pm 6.4	43.3 \pm 4.1	45.9 \pm 20.9	56 \pm 4.0	45.9 \pm 11.0	40.9 \pm 7.1	31.2 \pm 15.7	70.5 \pm 7.4	45.4 \pm 13.3	63.7 \pm 3.5	59.2 \pm 11.1	37.5 \pm 0.4
	CEM	65.8 \pm 15.0	43.3 \pm 4.1	57.3 \pm 14.4	56 \pm 4.0	36.6 \pm 15.8	40.9 \pm 7.1	39.0 \pm 10.8	70.5 \pm 7.4	43.3 \pm 17.8	63.7 \pm 3.5	65.2 \pm 2.1	37.5 \pm 0.4
	CGM	67.4 \pm 8.4	43.3 \pm 4.1	50.5 \pm 16.0	56 \pm 4.0	36.6 \pm 17.5	40.9 \pm 7.1	32.1 \pm 14.1	70.5 \pm 7.4	38.1 \pm 8.8	63.7 \pm 3.5	63.1 \pm 0.1	37.5 \pm 0.4
	C ² BM	61.9 \pm 19.2	43.3 \pm 4.1	43.2 \pm 24.6	56 \pm 4.0	36.1 \pm 17.9	40.9 \pm 7.1	22.2 \pm 23.3	70.5 \pm 7.4	36.7 \pm 7.8	63.7 \pm 3.5	63.1 \pm 0.1	37.5 \pm 0.4
S-F-CMs	OpaqNN	71.6 \pm 16.2	43.3 \pm 8	59.8 \pm 19.3	56 \pm 7.8	49.3 \pm 20.5	68.7 \pm 11.9	64.9 \pm 14.7	83.2 \pm 5.1	50.7 \pm 19.9	84.7 \pm 5.5	65.1 \pm 2.5	65 \pm 9.2
	CBM	59.9 \pm 11.0	43.3 \pm 8	50.9 \pm 26.1	56 \pm 7.8	41.3 \pm 21.0	68.7 \pm 11.9	58.5 \pm 23.3	83.2 \pm 5.1	57.3 \pm 17.9	84.7 \pm 5.5	62.9 \pm 12.8	65 \pm 9.2
	CEM	68.1 \pm 14.7	43.3 \pm 8	55.0 \pm 26.2	56 \pm 7.8	44.1 \pm 23.1	68.7 \pm 11.9	68.8 \pm 6.4	83.2 \pm 5.1	51.8 \pm 21.2	84.7 \pm 5.5	64.7 \pm 2.4	65 \pm 9.2
	CGM	67.1 \pm 14.4	43.3 \pm 8	44.0 \pm 28.8	56 \pm 7.8	52.6 \pm 18.5	48.7 \pm 20.6	57.9 \pm 23.0	76.8 \pm 11.6	42.9 \pm 14.8	84.7 \pm 5.5	63.2 \pm 0.2	65 \pm 9.2
	C ² BM	59.7 \pm 20.2	43.3 \pm 8	59.8 \pm 26.5	56 \pm 7.8	43.5 \pm 23.1	48.7 \pm 20.6	63.0 \pm 21.5	76.8 \pm 11.6	54.5 \pm 21.8	84.7 \pm 5.5	62.7 \pm 12.7	65 \pm 9.2
F-CMs	OpaqNN	80.0\pm1.8	100	75.1\pm2.1	100	72.9\pm0.5	100	71.8\pm2.3	100	66.0\pm3.4	100	67.1\pm2.4	100
	CBM	79.8\pm1.4	100	75.3\pm2.0	100	71.5\pm3.8	100	69.5\pm1.1	100	72.4\pm3.6	100	71.0\pm0.2	100
	CEM	80.5\pm1.7	100	76.0\pm2.6	100	73.4\pm0.4	100	71.0\pm0.8	100	70.2\pm3.8	100	67.3\pm2.7	100
	CGM	80.0\pm2.0	100	70.2\pm3.2	100	69.1\pm5.9	100	70.8\pm2.3	100	55.5\pm2.9	99.5\pm0.5	66.1\pm1.9	100
	C ² BM	80.4\pm2.2	100	76.2\pm2.1	100	73.1\pm0.8	100	74.3\pm2.3	100	72.8\pm2.1	99.5\pm0.5	68.8\pm2.5	100

Bayesian network benchmarks from bnlearn (Scutari, 2010) (ASIA (Lauritzen & Spiegelhalter, 1988), SACHS (Sachs et al., 2005), INSURANCE (Binder et al., 1997), ALARM (Beinlich et al., 1989), and HAILFINDER (Abramson et al., 1996)), each providing a ground-truth DAG. For real-world experiments, we use the SIIM-PNEUMOTHORAX dataset (You et al., 2023a), containing chest X-ray images labeled for pneumothorax, with concept annotations generated using a medical pre-trained CLIP model. For each dataset, we designate one variable as the task label Y and treat the remaining variables as concepts. In the centralized setting, graph-based models use the ground-truth DAG (or a proxy), while in federated and localized settings clients observe only subgraphs of the global structure and have access to local concept annotations. To model imperfect local knowledge (or data poisoning), client graphs are perturbed by randomly adding, removing, or reversing a subset of edges. See Appendices B, and D.1 for full details.

5.1. Task and Concept Coverage

We evaluate *task accuracy* and *concept coverage*, defined as the fraction of task-relevant concepts predicted by the model (i.e., concepts with a directed path to the task in the ground-truth DAG). Concept accuracy on predicted concepts is reported in Appendix E.1. To compare models with different coverage, variables not predicted by a model are treated as random guesses when computing accuracy. Table 1 reports results across CMs and training regimes across five runs.

Federated aggregation is necessary under statistical heterogeneity. Comparing S-F-CMs to Localized isolates the effect of cross-client aggregation when the concept space is fixed. Across benchmarks, S-F-CMs improves task accuracy and coverage over localized training, showing that aggregat-

ing supervision and (for graph-based models) structure is essential to reconcile heterogeneous client information.

But aggregation alone is insufficient under temporal non-stationarity; F-CMs close the gap. Under temporal non-stationarity, late-arriving clients introduce additional supervision (and, for graph-based models, new dependencies), so a fixed architecture becomes mismatched to the evolving concept space. This is reflected by the gap between S-F-CMs and both Centralized and F-CMs. By continuously extending the global concept set and updating the dependency graph, F-CMs can *adapt the shared architecture* and remain close to the centralized upper bound in task accuracy, while attaining near-100% coverage of task-relevant concepts.³ Appendix E.1 further shows that concept accuracy of F-CMs remains comparable to centralized training.

Overall, these results show that realistic federations require both (i) federated graph aggregation to handle heterogeneity and (ii) structure-aware architecture adaptation to sustain performance and interpretability as the federation evolves.

5.2. Concept-Level Interventions

After training each method under each learning regime, we evaluate responsiveness to *ground-truth concept interventions* by replacing an increasing number of predicted concepts with their ground-truth values, mimicking human corrections at deployment. To ensure a consistent intervention policy, interventions are sampled within progressively deeper levels in the hierarchy induced by the ground-truth DAG (or its proxy when it is unavailable). Figure 2 reports,

³The slight drop is due to imperfections in the aggregated graph, which can slightly affect the architecture. However, our analysis in Appendix D indicates that it is largely invariant to such noise.

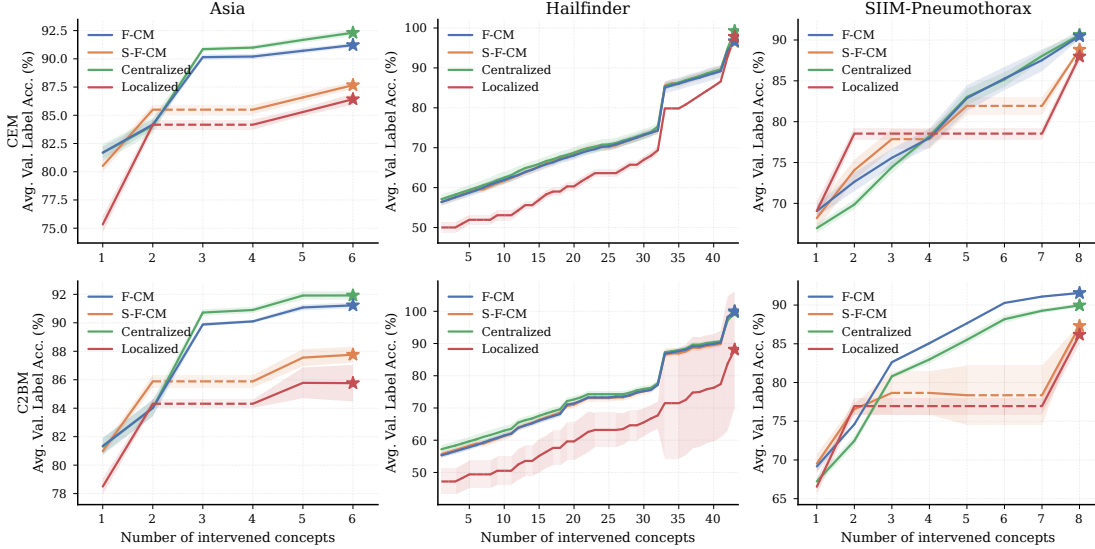


Figure 2. Label accuracy (%) on downstream variables (including the task) following interventions on concepts at deeper levels of the ground-truth graph hierarchy. Dashed lines denote interventions that are **not** possible for a given modality due to the absence of predictions for the corresponding concept.

after each intervention, the average accuracy over the remaining predicted variables (concepts and task), which we refer to as *label accuracy*, on three datasets (ASIA, HAILFINDER, and SIIM-PNEUMOTHORAX) and two representative CM instantiations (C^2BM and CEM). For clearer visualization we fix the client subgraphs across three seeds, isolating intervention effects from variability in the federated partition. Additional results are in Appendix E.

F-CMs enable interventions on locally unannotated concepts. Dashed segments mark interventions that are impossible because the corresponding concepts are *not predicted* by a given regime. This is visible for both Localized and S-F-CMs: localized models cannot predict concepts outside a client’s subgraph, while static federation can pool supervision and thus predict more concepts, but it fixes the concept space early and cannot incorporate concepts introduced by late clients. By combining cross-client aggregation with dynamic expansion/rewiring, F-CMs predict the broadest set of concepts and keep benefiting from further interventions, yielding higher label accuracy. The same trend holds for task accuracy alone (see Appendix E.2.1).⁴

F-CMs match centralized interventional responsiveness. Across datasets and architectures, F-CMs achieve accuracy comparable to centralized setting throughout the intervention trajectory, showing that our methodology preserves gains from concept corrections as pooled training does.

⁴The localized regime shows higher variance because, with limited concept supervision, the model may encode information about unobserved concepts into the predicted ones; interventions overwrite these predictions, leading to less stable gains.

5.3. Efficient Adaptation in Non-Stationary Federations

We evaluate how F-CMs behave in *non-stationary* federations where new clients join or leave during training and introduce previously unseen concepts, requiring the shared model to expand. Figure 3 reports the average validation task loss over communication rounds on the same datasets and instantiations of the previous experiment. In particular, we compare: **F-CMs** (ours), **S-F-CMs** (ours without architecture adaptation), and **S-F-CMs Reinit** (re-training from scratch whenever new clients join).

Across all datasets and both architectures, F-CMs consistently achieve better and faster convergence. They reach lower task loss than S-F-CMs, and avoid the slow recovery of the re-initialization baseline. Beyond accuracy, these results show a clear gain in *training compute-efficiency* in evolving federations. By design, F-CMs adapt only the modules affected by newly introduced concepts or dependencies, resulting in sparse parameter changes (e.g., 8%–43% across settings), compared to 0% for S-F-CMs (which cannot incorporate new concepts) and 100% for S-F-CMs Reinit (full re-training). Full results on the fraction of parameters changed are reported in Appendix E.3. These results highlight that **modular architecture adaptation yields a substantially more convergence-efficient strategy** for continual federation growth, preserving previously learned knowledge while integrating new supervision.

6. Related works

Several extensions of CMs relax the need for fully observed concept supervision by handling missing or noisy concept

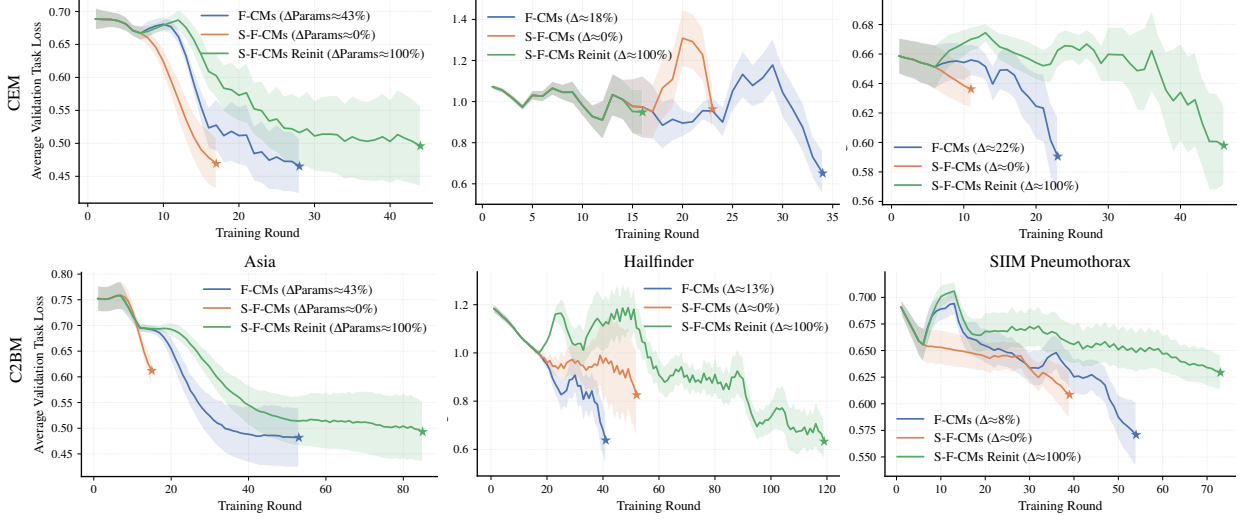


Figure 3. Convergence under temporal non-stationarity. Average validation task loss across rounds for C^2BM and CEM , where new clients introduce unseen concepts. F-CMs (ours) adapt the architecture modularly and converge faster and to lower loss than S-F-CMs (no adaptation) and S-F-CMs Reinit (full retraining). The legend reports the fraction of modified parameters.

labels and by combining supervised with unsupervised concept representations (Oikarinen et al., 2022; Sawada & Nakamura, 2022; Penalosa et al., 2025; Hu et al., 2025; Liu et al., 2025). However, these methods typically rely on pre-trained models to generate concept annotations, which must be tailored to the specific data domain to achieve accurate predictions. In contrast, our approach enables the use of ground-truth concept annotations, even when such annotations are distributed across multiple entities.

From the point of view of FL, integrating interpretability into FL is an emerging area of research. Recent works (Yang & Long, 2024; Shen et al., 2024; Zhang & Yu, 2024) take initial steps toward integrating concepts into the FL framework. However, these approaches do not rely on concept annotations; instead, concepts are extracted in an unsupervised manner (Kim et al., 2018; Wang et al., 2023). As a result, they cannot fully leverage FL to aggregate and exploit existing concept-level supervision across clients. Moreover, they typically assume a *static* federation: they do not address *temporal non-stationarity* in which new clients introduce previously unseen concepts and dependencies over time, requiring the global concept space—and potentially the architecture—to expand rather than remain fixed. Federated graph aggregation has been studied extensively in the context of *federated causal discovery*, which focus on discover causal relationships between variables from decentralized data. Existing methods typically assume a fixed (or pre-specified union) variable set across clients (Ng & Zhang, 2022; Huang et al., 2023; Li et al., 2024). However, this can be restrictive in realistic deployments with evolving concept sets, as in our setting. Moreover, our goal is a model-agnostic aggregation mechanism that is not tied

specifically to causal discovery. Beyond causal discovery, a large body of work studies *graph federated learning* (Zhang et al., 2021; He et al., 2021; Liu et al., 2024; Kim et al., 2025), which however focuses on training graph neural networks via federated optimization (i.e., aggregating model updates, and sometimes intermediate representations).

7. Conclusions

We introduced F-CMs, a novel methodology for training concept-based models in realistic federated settings under heterogeneous, partial concept supervision and temporal non-stationarity (dynamic participation and data drift). F-CMs aggregate concept supervision and, when available, concept dependencies across clients throughout training, while adapting the shared model modularly as the concept space evolves. Experiments show that F-CMs preserve task performance while improving concept coverage and intervention effectiveness over local and fixed federated architecture baselines. Importantly, F-CMs enable interpretable inference even for concepts that are locally unannotated.

Limitations and future work. Our approach assumes a shared input space and task across clients, which may limit applicability in federations with diverse modalities. While F-CMs can reuse existing CM architectures, these models were not designed for evolving concept spaces. A promising direction is to design federation-aware CMs with increased modularity, so that concept/dependency updates touch fewer parameters and yield even more efficient adaptation under temporal non-stationarity. We also plan to extend F-CMs to multimodal federations and strengthen the privacy analysis by systematically characterizing leakage and defenses.

Acknowledgements and Disclosure of Funding

This research was funded by the Swiss National Science Foundation, the European Union’s Horizon Europe programme, and the Slovenian Research and Innovation Agency through the projects SmartCHANGE (No. 101080965), TRUST-ME (No. 205121L_214991), and XAI-PAC (No. Z00P2_216405). AC and JS acknowledge support from FFF of the University of Liechtenstein grant lbs_24_08. PB acknowledges support from the Swiss National Science Foundation Postdoctoral Fellowships IMAGINE (No. 224226). GDF acknowledges support by the Swiss National Science Foundation (SNSF) through the grant 205121_197242 for the project “PROSELF: Semi-automated Self-Tracking Systems to Improve Personal Productivity” and the Hasler Foundation under the Project ID: 2024-05-15-70.

Impact Statement

This paper presents work aimed at advancing the field of machine learning. We expect F-CMs to facilitate the adoption of interpretable models, especially concept-based architectures, in privacy-sensitive domains such as healthcare, where data centralization is infeasible or legally constrained (e.g., under GDPR in Europe and, potentially, the California Consumer Privacy Act (CCPA) in the US, or the Personal Information Protection Law (PIPL) in China), and where concept annotations may be fragmented across institutions.

References

Abramson, B., Brown, J., Edwards, W., Murphy, A., and Winkler, R. L. Hailfinder: A bayesian system for forecasting severe weather. *International Journal of Forecasting*, 12(1):57–71, 1996.

Beinlich, I. A., Suermondt, H. J., Chavez, R. M., and Cooper, G. F. The ALARM Monitoring System: A Case Study with Two Probabilistic Inference Techniques for Belief Networks. In *Proceedings of the 2nd European Conference on Artificial Intelligence in Medicine*, pp. 247–256. Springer-Verlag, 1989. URL <https://www.cse.huji.ac.il/~galel/Repository/Datasets/alarm/alarm.htm>.

Binder, J., Koller, D., Russell, S., and Kanazawa, K. Adaptive probabilistic networks with hidden variables. *Machine Learning*, 29:213–244, 1997.

Chickering, D. M. Optimal structure identification with greedy search. *Journal of machine learning research*, 3 (Nov):507–554, 2002.

De Felice, G., Flores, A. C., De Santis, F., Santini, S., Schneider, J., Barbiero, P., and Termine, A. Causally reliable concept bottleneck models. *arXiv preprint arXiv:2503.04363*, 2025.

De Oliveira Jarczewski, R., Cerqueira, E., Bittencourt, L. F., A. F. Loureiro, A., A. Villas, L., and De Souza, A. M. Participation is Power: Effective Approach to Dynamic Federated Learning. In *Proceedings of the 18th IEEE/ACM International Conference on Utility and Cloud Computing, UCC ’25*, pp. 1–6. Association for Computing Machinery, December 2025. ISBN 979-8-4007-2285-1. doi: 10.1145/3773274.3774701.

Debole, N., Barbiero, P., Giannini, F., Passerini, A., Teso, S., and Marconato, E. If concept bottlenecks are the question, are foundation models the answer? *arXiv preprint arXiv:2504.19774*, 2025.

Dhar, T., Dey, N., Borra, S., and Sherratt, R. S. Challenges of deep learning in medical image analysis—improving explainability and trust. *IEEE Transactions on Technology and Society*, 4(1):68–75, 2023.

Dominici, G., Barbiero, P., Zarlenga, M. E., Termine, A., Gjoreski, M., Marra, G., and Langheinrich, M. Causal Concept Graph Models: Beyond Causal Opacity in Deep Learning. In *The Thirteenth International Conference on Learning Representations*, October 2024.

Dwork, C. Differential privacy. In Bugliesi, M., Preneel, B., Sassone, V., and Wegener, I. (eds.), *Automata, Languages and Programming*, pp. 1–12, Berlin, Heidelberg, 2006. Springer Berlin Heidelberg. ISBN 978-3-540-35908-1.

Espinosa Zarlenga, M., Barbiero, P., Ciravegna, G., Marra, G., Giannini, F., Diligenti, M., Shams, Z., Precioso, F., Melacci, S., Weller, A., et al. Concept embedding models: Beyond the accuracy-explainability trade-off. *Advances in neural information processing systems*, 35: 21400–21413, 2022.

Fenoglio, D., Dominici, G., Barbiero, P., Tonda, A., Gjoreski, M., and Langheinrich, M. Federated Behavioural Planes: Explaining the Evolution of Client Behaviour in Federated Learning. *Advances in Neural Information Processing Systems*, 37:112777–112813, 2024.

Fenoglio, D., Li, M., Barbiero, P., Lane, N. D., Langheinrich, M., and Gjoreski, M. FLUX: Efficient Descriptor-Driven Clustered Federated Learning under Arbitrary Distribution Shifts. In *The Thirty-ninth Annual Conference on Neural Information Processing Systems*, October 2025.

He, C., Balasubramanian, K., Ceyani, E., Yang, C., Xie, H., Sun, L., He, L., Yang, L., Yu, P. S., Rong, Y., et al. Fedgraphnn: A federated learning system and benchmark for graph neural networks. *arXiv preprint arXiv:2104.07145*, 2021.

Hu, L., Huang, T., Xie, H., Gong, X., Ren, C., Hu, Z., Yu, L., Ma, P., and Wang, D. Semi-supervised Concept Bottleneck Models. In *Proceedings of the IEEE/CVF International Conference on Computer Vision*, pp. 2110–2119, 2025.

Huang, J., Guo, X., Yu, K., Cao, F., and Liang, J. Towards privacy-aware causal structure learning in federated setting. *IEEE Transactions on Big Data*, 9(6):1525–1535, 2023.

Hurst, A., Lerer, A., Goucher, A. P., Perelman, A., Ramesh, A., Clark, A., Ostrow, A., Welihinda, A., Hayes, A., Radford, A., et al. Gpt-4o system card. *arXiv preprint arXiv:2410.21276*, 2024.

Jarczewski, R. O., Cerqueira, E., Bittencourt, L. F., Loureiro, A. A. F., Villas, L. A., and de Souza, A. M. Let's Federate - Effective Communication Strategy for Dynamic Client Participation. In *2024 International Conference on Machine Learning and Applications (ICMLA)*, pp. 361–368, December 2024. doi: 10.1109/ICMLA61862.2024.00055.

Jothimurugesan, E., Hsieh, K., Wang, J., Joshi, G., and Gibbons, P. B. Federated Learning under Distributed Concept Drift. In *Proceedings of The 26th International Conference on Artificial Intelligence and Statistics*, pp. 5834–5853. PMLR, April 2023.

Kairouz, P., McMahan, H. B., Avent, B., Bellet, A., Bennis, M., Nitin Bhagoji, A., Bonawitz, K., Charles, Z., Cormode, G., Cummings, R., D’Oliveira, R. G. L., Eichner, H., El Rouayheb, S., Evans, D., Gardner, J., Garrett, Z., Gascón, A., Ghazi, B., Gibbons, P. B., Gruteser, M., Harchaoui, Z., He, C., He, L., Huo, Z., Hutchinson, B., Hsu, J., Jaggi, M., Javidi, T., Joshi, G., Khodak, M., Konecný, J., Korolova, A., Koushanfar, F., Koyejo, S., Lepoint, T., Liu, Y., Mittal, P., Mohri, M., Nock, R., Özgür, A., Pagh, R., Qi, H., Ramage, D., Raskar, R., Raykova, M., Song, D., Song, W., Stich, S. U., Sun, Z., Suresh, A. T., Tramèr, F., Vepakomma, P., Wang, J., Xiong, L., Xu, Z., Yang, Q., Yu, F. X., Yu, H., and Zhao, S. Advances and Open Problems in Federated Learning. *Found. Trends Mach. Learn.*, 14(1-2):1–210, June 2021. ISSN 1935-8237. doi: 10.1561/2200000083.

Kaassis, G. A., Makowski, M. R., Rückert, D., and Braren, R. F. Secure, privacy-preserving and federated machine learning in medical imaging. *Nature Machine Intelligence*, 2(6):305–311, June 2020. ISSN 2522-5839. doi: 10.1038/s42256-020-0186-1.

Kaminski, M. E. The right to explanation, explained. In *Research handbook on information law and governance*, pp. 278–299. Edward Elgar Publishing, 2021.

Kim, B., Wattenberg, M., Gilmer, J., Cai, C., Wexler, J., Viegas, F., et al. Interpretability beyond feature attribution: Quantitative testing with concept activation vectors (tcav). In *International conference on machine learning*, pp. 2668–2677. PMLR, 2018.

Kim, S., Lee, Y., Oh, Y., Lee, N., Yun, S., Lee, J., Kim, S., Yang, C., and Park, C. Subgraph federated learning for local generalization. *arXiv preprint arXiv:2503.03995*, 2025.

Koh, P. W., Nguyen, T., Tang, Y. S., Mussmann, S., Pierson, E., Kim, B., and Liang, P. Concept bottleneck models. In *International conference on machine learning*, pp. 5338–5348. PMLR, 2020.

Lauritzen, S. L. and Spiegelhalter, D. J. Local Computation with Probabilities on Graphical Structures and their Application to Expert Systems (with discussion). *Journal of the Royal Statistical Society: Series B (Statistical Methodology)*, 50(2):157–224, 1988.

Lewis, P., Perez, E., Piktus, A., Petroni, F., Karpukhin, V., Goyal, N., Küttler, H., Lewis, M., Yih, W.-t., Rocktäschel, T., et al. Retrieval-augmented generation for knowledge-intensive nlp tasks. *Advances in Neural Information Processing Systems*, 33:9459–9474, 2020.

Li, L., Ng, I., Luo, G., Huang, B., Chen, G., Liu, T., Gu, B., and Zhang, K. Federated causal discovery from heterogeneous data. In *The Twelfth International Conference on Learning Representations*, 2024.

Li, M., Fenoglio, D., Gjoreski, M., and Langheinrich, M. Federated Learning with Profile Mapping under Distribution Shifts and Drifts. In *The Fourteenth International Conference on Learning Representations*, October 2026.

Li, X., Xiong, H., Li, X., Wu, X., Zhang, X., Liu, J., Bian, J., and Dou, D. Interpretable deep learning: Interpretation, interpretability, trustworthiness, and beyond. *Knowledge and Information Systems*, 64(12):3197–3234, 2022.

Litjens, G., Bandi, P., Ehteshami Bejnordi, B., Geessink, O., Balkenhol, M., Bult, P., Halilovic, A., Hermsen, M., van de Loo, R., Vogels, R., Manson, Q. F., Stathonikos, N., Baidoshvili, A., van Diest, P., Wauters, C., van Dijk, M., and van der Laak, J. 1399 H&E-stained sentinel lymph node sections of breast cancer patients: The CAMELYON dataset. *GigaScience*, 7(6):giy065, June 2018. ISSN 2047-217X. doi: 10.1093/gigascience/giy065.

Liu, R., Xing, P., Deng, Z., Li, A., Guan, C., and Yu, H. Federated graph neural networks: Overview, techniques, and challenges. *IEEE transactions on neural networks and learning systems*, 2024.

Liu, Y., Zhang, T., and Gu, S. Hybrid Concept Bottleneck Models. In *Proceedings of the Computer Vision and Pattern Recognition Conference*, pp. 20179–20189, 2025.

McMahan, H. B., Moore, E., Ramage, D., Hampson, S., and y Arcas, B. A. Communication-Efficient Learning of Deep Networks from Decentralized Data, January 2023.

Ng, I. and Zhang, K. Towards federated bayesian network structure learning with continuous optimization. In *International Conference on Artificial Intelligence and Statistics*, pp. 8095–8111. PMLR, 2022.

Oikarinen, T., Das, S., Nguyen, L. M., and Weng, T.-W. Label-free Concept Bottleneck Models. In *The Eleventh International Conference on Learning Representations*, September 2022.

Panchal, K., Choudhary, S., Mitra, S., Mukherjee, K., Sarkhel, S., Mitra, S., and Guan, H. Flash: Concept Drift Adaptation in Federated Learning. *Fortieth International Conference on Machine Learning*, June 2023.

Pearl, J. Causal diagrams for empirical research. *Biometrika*, 82(4):669–688, 1995.

Penaloza, E., Zhang, T. H., Charlin, L., and Zarlenga, M. E. Addressing Concept Mislabeled in Concept Bottleneck Models Through Preference Optimization, September 2025.

Poeta, E., Ciravegna, G., Pastor, E., Cerquitelli, T., and Baralis, E. Concept-based explainable artificial intelligence: A survey. *ACM Computing Surveys*, 2023.

Sachs, K., Perez, O., Pe'er, D., Lauffenburger, D. A., and Nolan, G. P. Causal protein-signaling networks derived from multiparameter single-cell data. *Science*, 308(5721):523–529, 2005.

Sawada, Y. and Nakamura, K. Concept Bottleneck Model With Additional Unsupervised Concepts. *IEEE Access*, 10:41758–41765, 2022. ISSN 2169-3536. doi: 10.1109/ACCESS.2022.3167702.

Scutari, M. Learning bayesian networks with the bnlearn r package. *Journal of Statistical Software*, 35(i03), 2010.

Shen, J., Tao, X., Li, L., Li, Z., and Wang, B. Explaining Federated Learning Through Concepts in Image Classification. In Tari, Z., Li, K., and Wu, H. (eds.), *Algorithms and Architectures for Parallel Processing*, pp. 325–340, Singapore, 2024. Springer Nature. ISBN 978-981-97-0808-6. doi: 10.1007/978-981-97-0808-6_19.

Sun, G., Cong, Y., Dong, J., Wang, Q., Lyu, L., and Liu, J. Data Poisoning Attacks on Federated Machine Learning. *IEEE Internet of Things Journal*, 9(13):11365–11375, July 2022. ISSN 2327-4662. doi: 10.1109/JIOT.2021.3128646.

Wang, B., Li, L., Nakashima, Y., and Nagahara, H. Learning bottleneck concepts in image classification. In *Proceedings of the ieee/cvf conference on computer vision and pattern recognition*, pp. 10962–10971, 2023.

Xiang, M., Ioannidis, S., Yeh, E., Joe-Wong, C., and Su, L. Efficient Federated Learning against Heterogeneous and Non-stationary Client Unavailability. In *The Thirty-eighth Annual Conference on Neural Information Processing Systems*, November 2024.

Yang, J. and Long, G. Concept-Guided Interpretable Federated Learning. In Liu, T., Webb, G., Yue, L., and Wang, D. (eds.), *AI 2023: Advances in Artificial Intelligence*, pp. 160–172, Singapore, 2024. Springer Nature. ISBN 978-981-99-8391-9. doi: 10.1007/978-981-99-8391-9_13.

You, K., Gu, J., Ham, J., Park, B., Kim, J., Hong, E. K., Baek, W., and Roh, B. Cxr-clip: Toward large scale chest x-ray language-image pre-training. In *International Conference on Medical Image Computing and Computer-Assisted Intervention*, pp. 101–111. Springer, 2023a.

You, K., Gu, J., Ham, J., Park, B., Kim, J., Hong, E. K., Baek, W., and Roh, B. Cxr-clip: Toward large scale chest x-ray language-image pre-training. In *International Conference on Medical Image Computing and Computer-Assisted Intervention*, pp. 101–111. Springer, 2023b.

Yousefpour, A., Shilov, I., Sablayrolles, A., Testuggine, D., Prasad, K., Malek, M., Nguyen, J., Ghosh, S., Bharadwaj, A., Zhao, J., Cormode, G., and Mironov, I. Opacus: User-Friendly Differential Privacy Library in PyTorch, August 2022. Privacy in Machine Learning (PriML) workshop, NeurIPS 2021.

Zhang, K., Yang, C., Li, X., Sun, L., and Yiu, S. M. Subgraph federated learning with missing neighbor generation. *Advances in neural information processing systems*, 34:6671–6682, 2021.

Zhang, Y. and Yu, H. LR-XFL: Logical Reasoning-Based Explainable Federated Learning. *Proceedings of the AAAI Conference on Artificial Intelligence*, 38(19):21788–21796, March 2024. ISSN 2374-3468. doi: 10.1609/aaai.v38i19.30179.

A. Extended background

B. Dataset Details

B.1. Bayesian Network Datasets (bnlearn)

We consider five benchmark Bayesian networks from the `bnlearn` repository (Scutari, 2010), spanning diverse application domains and varying in graph size and structural complexity.

- *Asia*: A small network for lung disease diagnosis with 8 variables representing patient symptoms and conditions (smoking, tuberculosis, lung cancer, bronchitis, dyspnea, X-ray results, visits to Asia).
- *Sachs*: A widely used network capturing dependencies among protein and phospholipid expression levels in human cells.
- *Alarm*: A medical network designed to provide an alarm message system for patient monitoring.
- *Insurance*: A network for car insurance risk assessment with 27 variables covering driver characteristics, vehicle properties, and accident-related factors.
- *Hailfinder*: A weather forecasting network with 56 variables for predicting severe weather conditions in northeastern Colorado, including atmospheric measurements and storm indicators.

Table 2. Summary of bnlearn datasets used in experiments.

Dataset	Nodes	Edges	Domain
Asia	8	8	Medical diagnosis
Sachs	11	17	Protein signaling
Alarm	37	46	Medical monitoring
Insurance	27	52	Insurance risk
Hailfinder	56	66	Weather prediction

For each network, we generate a dataset with a network-specific number of samples, selected via preliminary experiments to ensure stable performance: 15,000 for Asia, 15,000 for Sachs, 10,000 for Alarm, 20,000 for Insurance, and 20,000 for Hailfinder. Each dataset is split into training, validation, and test sets using a standard 70%–10%–20% split. The networks are interpreted causally and their graphs are treated as ground truth. Nodes in each network are treated as concepts $\{C_j\}_j$ or as the task variable Y , yielding complete annotations, whereas the datasets do not natively include input features X . To construct inputs suitable for concept-based models, concept values are flattened and passed through a simple autoencoder trained with an MSE loss, consisting of two encoder and two decoder layers. The latent dimensionality is scaled with graph size (Asia: 32, Sachs: 32, Insurance: 64, Alarm: 64, Hailfinder: 64). The resulting embeddings are further perturbed by mixing 50% of the encoded signal with 50% Gaussian noise, and the final inputs are standardized. These transformations yield non-trivial input representations, requiring models to recover the underlying concepts rather than trivially accessing them. Tasks chosen in the experiment are respectively: dysp (Asia), Akt (Sachs), PropCost (Insurance), BP (Alarm), R5Fest (Hailfinder).

B.2. SIIM-Pneumothorax

This dataset consists of chest X-ray images with binary labels indicating the presence or absence of pneumothorax, released by the National Institutes of Health (NIH). For our experiments, we use the training images and annotations from the SIIM-ACR Pneumothorax Segmentation challenge hosted on Kaggle (<https://www.kaggle.com/competitions/siim-acr-pneumothorax-segmentation>; <https://www.kaggle.com/datasets/abhishek/siim-png-images>) and split the data into training, validation, and test sets using a standard 70%–10%–20% partition. As the dataset does not provide concept-level annotations, we generate concept labels using a pretrained medical imaging model (CXR-CLIP) (You et al., 2023b), following the methodology of Oikarinen et al. (2022).

C. Baseline details

All the baselines considered share the same input encoder. They differ only in the parameterization of the concept predictors and the task decoder, and in whether they use a bipartite graph (CBM/CEM) or a more general DAG \mathcal{G} connecting concepts and task.

Concept Bottleneck Models (CBMs) (Koh et al., 2020). CBMs use a bipartite graph. Specifically, each concept is predicted independently from an encoder representation:

$$\hat{c}_j = h_{\phi_j}(z), \quad j \in \mathcal{M},$$

where h_{ϕ_j} is an MLP head outputting either logits/probabilities (categorical concepts) or real values (continuous concepts). The task decoder operates only on the predicted concepts,

$$\hat{y} = f_{\psi}(\hat{c}_{\mathcal{M}}),$$

implemented as an MLP over the concatenation of all concept predictions (no direct dependence on z).

Concept Embedding Models (CEMs) (Espinosa Zarlenga et al., 2022). CEMs share the same bipartite construction as CBMs, but represent each concept with an embedding rather than a scalar. For each concept j , the model first produces two concept-specific embeddings from the encoder representation z :

$$\hat{c}_j^+ = \varphi_{\phi_j}^+(z) \in \mathbb{R}^r, \quad \hat{c}_j^- = \varphi_{\phi_j}^-(z) \in \mathbb{R}^r,$$

where \hat{c}_j^+ encodes the *active* state and \hat{c}_j^- the *inactive* state of concept C_j . Then, a scoring function maps their joint space to a concept activity probability,

$$\hat{p}_j = s_{\phi}([\hat{c}_j^+, \hat{c}_j^-]^T) = \sigma(W_s[\hat{c}_j^+, \hat{c}_j^-]^T + b_s) \in [0, 1],$$

and the final concept embedding fed to the task is the corresponding mixture:

$$\tilde{c}_j = \hat{p}_j \hat{c}_j^+ + (1 - \hat{p}_j) \hat{c}_j^- \in \mathbb{R}^r.$$

The task decoder then operates on the concatenation of mixed concept embeddings $\hat{c}_{\mathcal{M}}$,

$$\hat{y} = f_{\psi}(\hat{c}_{\mathcal{M}}),$$

implemented as an (interpretable) linear layer or a small MLP.

Fed-CGM (CGM) (Dominici et al., 2024). We implement CGMs using the aggregated DAG produced by our methodology. For each concept node C_j , we predict

$$\hat{c}_j = h_{\phi,j}(\hat{c}_{\text{PA}(C_j)}, z),$$

where $h_{\phi,j}$ is an MLP that takes as input the concatenation of its parent \tilde{c} concept embedding computed using \hat{c} and the encoder representation z , in a similar format as CEM. The task prediction is computed analogously,

$$\hat{y} = f_{\psi}(\hat{c}_{\text{PA}(Y)}, z).$$

This factorization ensures that changes to upstream concepts propagate to downstream concepts and the task through the parent-conditioned modules.

Causally Reliable Concept Bottleneck Models (C²BMs) (De Felice et al., 2025). C²BMs also use our aggregated DAG, but explicitly separate *exogenous* information extracted from the input from the *structural* mechanism mapping parent variables to each node.

Concretely, each node V in the DAG is equipped with a CEM-style module that outputs an embedding u_V representing the node-specific exogenous signal extracted from the input. This exogenous representation is used (a) to predict *root* nodes

directly via a lightweight output head, and (b) to *parameterize* the parent-to-node mechanism for *non-root* nodes through a hypernetwork. In particular, for non-root nodes we first generate node-specific coefficients from u_V ,

$$\theta_V = r_{\phi_V}(u_V),$$

and then predict V from its parents with a linear-in-parents map followed by the appropriate output nonlinearity:

$$\hat{V} = \sigma_V \left(\langle \theta_V, \hat{V}_{\text{PA}(V)} \rangle + b_V \right) \equiv f_{\theta_V}(\hat{V}_{\text{PA}(V)}),$$

where r_{ϕ_V} is an MLP (hypernetwork) and σ_V is chosen according to the variable type (e.g., sigmoid/softmax/identity). The task node Y is treated identically as a node in the graph.

D. Experimental details

D.1. Details on data preparation

SIIM-Pneumothorax ground-truth graph. The ground-truth graph among concepts and the task for SIIM-Pneumothorax is constructed following a procedure similar to the one provided in [De Felice et al. \(2025\)](#). First, the Greedy Equivalence Search (GES) algorithm ([Chickering, 2002](#)), a causal discovery method that infers causal structure from observational data, is applied to the concept and task annotations to produce an initial graph. This graph however may still contain unoriented edges. To resolve these ambiguities, we employ a large language model (LLM), specifically GPT-4○ ([Hurst et al., 2024](#)), enhanced with retrieval-augmented generation (RAG) ([Lewis et al., 2020](#)), which uses domain-specific medical literature to provide context. This process enriches the initial graph with background knowledge, yielding the final DAG.

Client local data. In our setting, each client k holds a local dataset

$$\mathcal{D}^{(k)} := \{(x_i^{(k)}, c_i^{(k)}, y_i^{(k)})\}_{i=1}^{n^{(k)}},$$

where $x_i^{(k)}$ is the input, $c_i^{(k)}$ are concept annotations (possibly partial or missing), and $y_i^{(k)}$ is the task label (possibly missing). A client may also provide a local DAG $\mathcal{G}^{(k)}$ encoding relationships among its observed concepts and (when available) the task.

For our experiments, we generate client data as follows. Given a dataset \mathcal{D} with full inputs, concepts, and task annotations, a DAG \mathcal{G} , and a set of K clients, we first construct K subgraphs $\{\mathcal{G}^{(k)}\}_{k=1}^K$ of \mathcal{G} . Each subgraph is built as follows: starting from the task node Y (a leaf in the graph \mathcal{G}), we repeatedly move *upstream* by following incoming edges and collect multiple ancestor paths up to the roots; we then take the union of these paths (equivalently, the induced ancestor tree of Y). To increase heterogeneity across clients, we additionally sample a set of random concepts nodes that are not contained in the set of roots of \mathcal{G} and, for each of them, collect one or more ancestor paths up to the roots; these paths are finally merged with the subgraph built from Y . The task node Y is then randomly excluded from a subset of clients to model missing task supervision. We ensure total concept coverage, i.e., the union of client subgraphs contains all concepts and task. To simulate imperfect client knowledge of concept relations, we perturb each $\mathcal{G}^{(k)}$ by modifying a fraction p of its edges (configuration parameter) for a percentage r of clients. Specifically, for these clients, we randomly flip, remove or add edges to their DAGs while preserving acyclicity. The resulting aggregated $\mathcal{G}^{(k)}$ is the graph provided to the server.

Local datasets are then obtained by partitioning \mathcal{D} into K disjoint subsets of approximately equal size. For client k , we retain only the supervision available in its subgraph, i.e., for the concepts and/or the task contained in the set of nodes of the subgraph. All other concept and task are treated as unobserved for that client.

D.2. Algorithm

Algorithm 1 summarizes the end-to-end F-CMs training loop under statistical heterogeneity and temporal non-stationarity. At each round, the server samples available clients, aggregates their reported concept indices (and optional local structure) into an updated shared concept set and DAG, and then adapts the shared CM architecture modularly. Clients perform module-specific local updates by freezing unsupervised components, and the server aggregates updates module-wise, averaging each module only over clients that contributed to it.

Algorithm 1 F-CMS: Federated Concept-based Models.

Input: Initial shared parameters $\mathbf{w}_0 = (\theta_0, \phi_0, \psi_0)$, concept set \mathcal{M}_0 , shared DAG \mathcal{G}_0 (optional), number of rounds T
Output: Final shared model parameters $\mathbf{w}_T = (\theta_T, \phi_T, \psi_T)$ and shared structure $(\mathcal{M}_T, \mathcal{G}_T)$

```

1 for  $t = 0, 1, \dots, T - 1$  do
2    $\mathcal{K}_t \leftarrow \text{CLIENTSAMPLING}(\mathcal{K}(t))$ 
   // Client-side: local graph proposals
3   for each client  $k \in \mathcal{K}_t$  in parallel do
4     if  $k$  has local structure information then
5       Send  $S^{(k)}$  (or  $\mathcal{A}^{(k)}$ ) and  $n^{(k)}$  to server
6     Send observed concept index set  $I^{(k)}$ 
7   // Server-side: shared structure update
8    $\mathcal{M}_t \leftarrow \mathcal{M}_{t-1} \cup \bigcup_{k \in \mathcal{K}_t} I^{(k)}$ 
9    $\mathcal{G}_t \leftarrow \text{AGGREGATEDAG}(\{S^{(k)}\}_{k \in \mathcal{K}_t}, \{\alpha_k\})$ 
10   $\tilde{\mathbf{w}}_t \leftarrow \text{ADAPTMODEL}(\mathbf{w}_t, \mathcal{M}_t, \mathcal{G}_t)$ 
11  Broadcast  $(\tilde{\mathbf{w}}_t, \mathcal{G}_t, \mathcal{M}_t)$  to all clients in  $\mathcal{K}_t$ 
12  // Client-side: module-specific training
13  for each client  $k \in \mathcal{K}_t$  in parallel do
14     $\tilde{\mathbf{w}}_t^{(k)} \leftarrow \text{FREEZEUNSUP}(\tilde{\mathbf{w}}_t, \mathcal{G}_t, I^{(k)}, k \in \mathcal{K}_t^Y)$ 
15     $\Delta\tilde{\mathbf{w}}_t^{(k)} \leftarrow \text{LOCALUPDATE}(\tilde{\mathbf{w}}_t, \mathcal{G}_t, I^{(k)}, \mathcal{D}^{(k)})$ 
     Send  $\Delta\tilde{\mathbf{w}}_t^{(k)}$  to server
16  // Server-side: module-wise aggregation
17   $\mathbf{w}_{t+1} \leftarrow \text{MODULEWISEFEDAVG}(\tilde{\mathbf{w}}_t, \{\Delta\tilde{\mathbf{w}}_t^{(k)}\}_{k \in \mathcal{K}_t})$ 

```

D.3. Training Details

Optimization and initialization. All models are trained using the Adam optimizer with LeakyReLU activations throughout. Experiments are repeated over different random seeds, affecting data partitioning, client assignment, and model initialization. The batch size is fixed to 512 across all datasets and learning regimes. All models use the loss defined in Eq. (2), with the concept–task trade-off parameter set to $\gamma = 0.8$. Key hyperparameters—including learning rate, MLP hidden dimension, and dropout rate—are tuned via grid search on validation sets independently for each dataset and model. Complete hyperparameter configurations for all methods and training regimes are provided in the YAML configuration files released with the code. During training, we apply random concept interventions with probability 0.25, following the protocol of Espinosa Zarlena et al. (2022), to encourage robustness to concept-level corrections.

Centralized and localized training. For centralized and localized baselines, models are trained for up to 200 epochs with early stopping based on the validation loss, using a patience of 10 epochs without improvement. To ensure a fair comparison with federated methods, we control for the total amount of training data. In the centralized setting, we train on the union of all data available across the federation over time, i.e., pooling the datasets of all clients that appear in $\mathcal{K}(t)$ throughout training. In the localized setting, each model is trained using data from a single client; the number of localized models equals the size of the largest client pool.

Federated training. Federated methods are trained for up to 200 communication rounds. At each round, clients perform 2 local epochs before sending updates to the server. Early stopping is applied based on the global validation loss, with a patience of 10 rounds without improvement. Unless otherwise specified (e.g., when varying the number of clients in Section E.5.1), the number of participating clients per round is fixed to $|\mathcal{K}_t| = 10$ across all experiments. All federated experiments are conducted under *dynamic client participation* (and resulting data drift). The client pool $\mathcal{K}(t)$ evolves over time, reaching a total of 20 clients. After an initial warm-up phase—at round $t = 10$ for ASIA, SACHS, and SIIM, and at $t = 20$ for the remaining datasets—new clients join the federation. These late-arriving clients introduce additional concept supervision and, for graph-based instantiations, potentially novel dependency structures. Following client introduction, the client pool is balanced such that approximately 50% of clients belong to the initial data distribution and 50% to the new distribution.

Parameter freezing under partial supervision. To enforce *module-specific training* under partial concept/task supervision (Section 4.2.3), each client updates only the modules it can directly supervise. Concretely, concept (and task) labels may

Table 3. Concept Accuracy.

Setting	Model	Asia	Sachs	Alarm	Insurance	Hailfinder	SIIM Pn.
Cent. (Upper Bound)	OpaqNN	91.6 \pm 0.7	75.1 \pm 1.1	91.3 \pm 0.1	79.6 \pm 0.5	58.4 \pm 1.2	74.6 \pm 0.3
	CBM	91.5 \pm 0.8	74.8 \pm 1.3	91.2 \pm 0.1	79.6 \pm 0.4	69.0 \pm 0.7	74.5 \pm 0.3
	CEM	91.4 \pm 0.7	73.9 \pm 0.7	90.1 \pm 0.5	77.1 \pm 0.5	61.7 \pm 0.8	73.2 \pm 0.3
	CGM	91.1 \pm 0.9	72.5 \pm 1.2	89.3 \pm 0.4	72.2 \pm 0.4	60.6 \pm 1.7	65.9 \pm 1.7
	C ² BM	91.2 \pm 0.8	74.5 \pm 0.9	90.5 \pm 0.6	77.5 \pm 0.4	62.8 \pm 1.2	72.9 \pm 0.4
Loc.	OpaqNN	66.5 \pm 6.5	53.2 \pm 2.6	63.1 \pm 7.8	63.3 \pm 5.6	42.7 \pm 3.3	58.4 \pm 3.0
	CBM	66.6 \pm 6.6	52.8 \pm 2.9	63.7 \pm 7.6	64.0 \pm 5.5	46.3 \pm 2.8	58.9 \pm 3.0
	CEM	65.5 \pm 6.8	49.8 \pm 3.3	62.7 \pm 7.7	63.4 \pm 5.4	42.6 \pm 5.5	57.2 \pm 2.5
	CGM	65.9 \pm 7.0	48.5 \pm 1.2	56.8 \pm 7.4	56.4 \pm 5.7	39.2 \pm 3.1	54.8 \pm 1.1
	C ² BM	66.2 \pm 6.8	49.8 \pm 1.7	57.0 \pm 7.5	60.2 \pm 6.0	39.1 \pm 4.5	54.6 \pm 1.3
S-F-CMs	OpaqNN	67.6 \pm 5.9	56.0 \pm 3.0	73.8 \pm 5.8	69.9 \pm 3.3	51.5 \pm 0.7	59.7 \pm 2.1
	CBM	67.8 \pm 5.9	56.6 \pm 3.3	74.5 \pm 5.6	71.4 \pm 3.5	60.8 \pm 0.9	61.9 \pm 1.5
	CEM	67.7 \pm 5.9	56.0 \pm 3.2	74.1 \pm 5.7	69.7 \pm 3.4	55.9 \pm 0.9	59.4 \pm 1.6
	CGM	67.3 \pm 5.9	54.8 \pm 2.6	62.7 \pm 11.0	63.5 \pm 5.6	51.6 \pm 1.7	57.9 \pm 1.3
	C ² BM	67.6 \pm 5.9	55.8 \pm 3.1	63.1 \pm 11.1	66.1 \pm 6.0	54.3 \pm 1.1	61.3 \pm 1.7
F-CMs	OpaqNN	91.1 \pm 0.9	72.9 \pm 1.3	90.2 \pm 0.2	77.2 \pm 0.7	53.6 \pm 0.7	63.4 \pm 1.8
	CBM	91.1 \pm 0.9	74.1 \pm 1.1	90.5 \pm 0.3	78.8 \pm 0.9	65.4 \pm 0.4	68.9 \pm 0.6
	CEM	89.8 \pm 2.0	73.0 \pm 1.4	90.1 \pm 0.6	77.2 \pm 0.7	60.1 \pm 1.3	64.9 \pm 1.6
	CGM	89.5 \pm 1.8	69.3 \pm 1.5	88.8 \pm 1.6	72.4 \pm 1.6	52.8 \pm 2.1	63.7 \pm 1.5
	C ² BM	90.6 \pm 1.0	72.2 \pm 1.7	90.2 \pm 0.3	76.1 \pm 1.2	57.7 \pm 1.4	67.7 \pm 1.3

be missing at a client, which we represent via a missing-label mask (e.g., value -1). At the start of local training for client k , we identify the supervised concept index set $I^{(k)} = \{j : c_j^{(k)} \text{ is observed}\}$ and whether the task label is available (i.e., $k \in \mathcal{K}_Y$). We then *freeze* all concept modules $h_{\phi,j}$ with $j \notin I^{(k)}$, and freeze the task module f_ψ whenever $k \notin \mathcal{K}_Y$. This mechanism applies uniformly across instantiations (CBM/CEM/C²BM): regardless of parameterization, any module without local supervision is held fixed during the client update, while only supervised modules (and the shared encoder) are optimized. As a result, local updates match Eq. (2) by preventing gradients from modifying unsupervised components, and naturally supports module-wise aggregation since clients return updates only for the modules they trained.

E. Additional Experiments

E.1. Concept Accuracy

We report concept accuracy as the average accuracy across all concepts (no downstream task), evaluated in the same experimental setting as Section 5.1. Across benchmarks, our method closely remain close to the centralized upper bound. Under the adopted protocol, where unsupported concepts are assigned random predictions, our higher average concept accuracy indicates that our method maintains high performance even when accounting for concepts that cannot be predicted by Localized and S-F-CMs baselines.

E.2. Concept-Level Interventions - Further Experiments

E.2.1. TASK ACCURACY

We report the task accuracy of the C²BM and CEM instantiations of F-CMs, evaluated under the same experimental setup as in Section 5.2. The results are consistent with the findings discussed in that section.

E.2.2. COMPARISON OF F-CMs INSTANTIATIONS

We further compare how different CM instantiations benefit from the proposed federated protocol by evaluating performance under concept-level interventions. Figures 5 and 6 report, respectively, the *label accuracy* and *task accuracy* obtained after intervening on concepts sampled at increasing depths of the ground-truth hierarchy (Section 5.2). Overall, both metrics exhibit consistent trends: improvements in corrected concept predictions translate into accuracy gains, with larger gains typically obtained when intervening on upstream concepts.

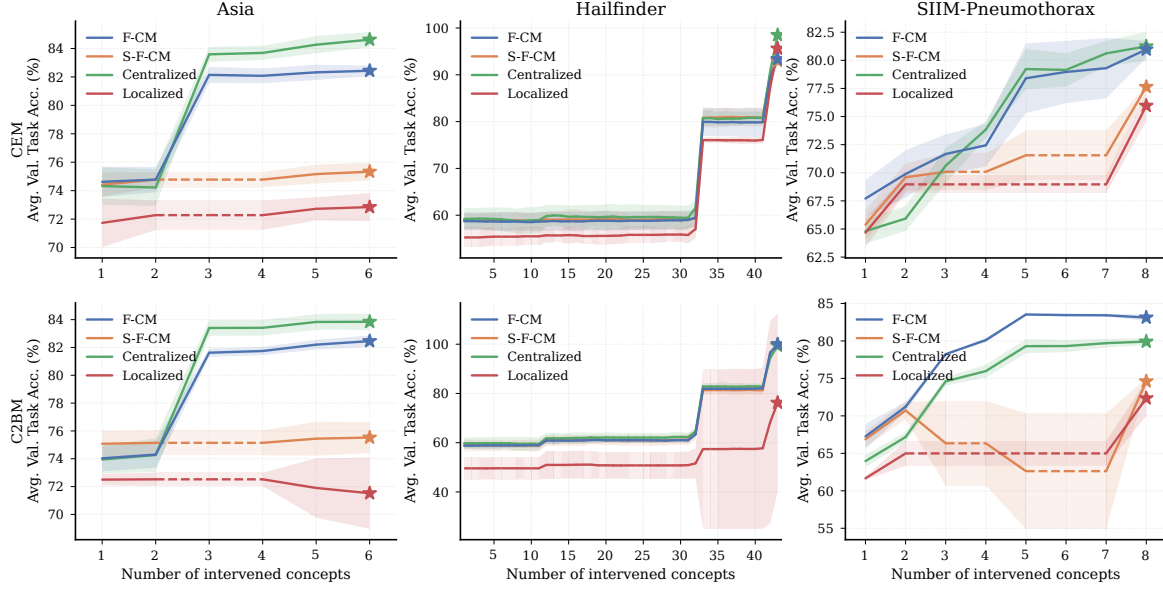


Figure 4. Task accuracy (%) following interventions on concepts at increasing depths of the ground-truth graph hierarchy. Dashed lines denote interventions that are not possible for a given modality due to the absence of predictions for the corresponding concept.

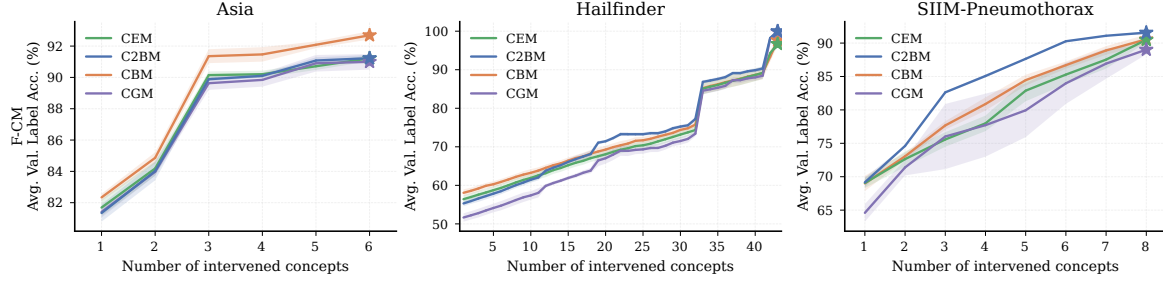


Figure 5. Label accuracy (%) following interventions on concepts at increasing depths of the ground-truth graph hierarchy across CMs instantiations.

On ASIA, the bipartite CBM variant often shows the strongest response to interventions. We attribute this to the small scale and limited structural complexity of ASIA: when the concept set is compact and most concepts have short causal paths to the task, explicitly modeling concept dependencies offers limited additional benefit, while the simpler bipartite parameterization can be easier to optimize and less sensitive to graph misspecification. On the larger and more structurally rich datasets (HAILFINDER and SIIM-PNEUMOTHORAX), graph-based instantiations—especially C²BM—tend to yield stronger gains under interventions. In these settings, leveraging concept-to-concept relations allows corrected upstream concepts to propagate through parent-conditioned predictors, improving downstream concepts and ultimately the task.

E.2.3. DIFFERENT MODELS

We repeated the experiments of Section 5.2 and Appendix E.2.1 using different model architectures. Specifically, we report both label and task accuracy for the F-CM instantiations not previously shown (CBM and CGM), evaluated under the same experimental setup as in Section 5.2. The results are consistent with the findings discussed in that section.

E.3. Extent of Architecture Updates Under Temporal Non-Stationarity

To quantify the efficiency of *dynamic architecture adaptation* under temporal non-stationarity, we measure the fraction of shared model parameters whose values change after new clients introduce previously unseen concepts (and, for graph-based instantiations, updated dependencies). Concretely, we report the percentage of parameters that differ between the shared model before the arrival of new clients and the final shared model at the end of training, averaged across seeds. We use this

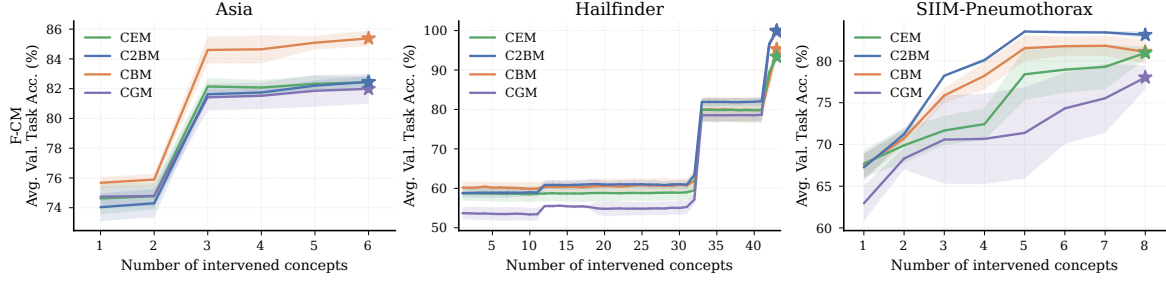


Figure 6. Task accuracy (%) following interventions on concepts at increasing depths of the ground-truth graph hierarchy across CMs instantiations.

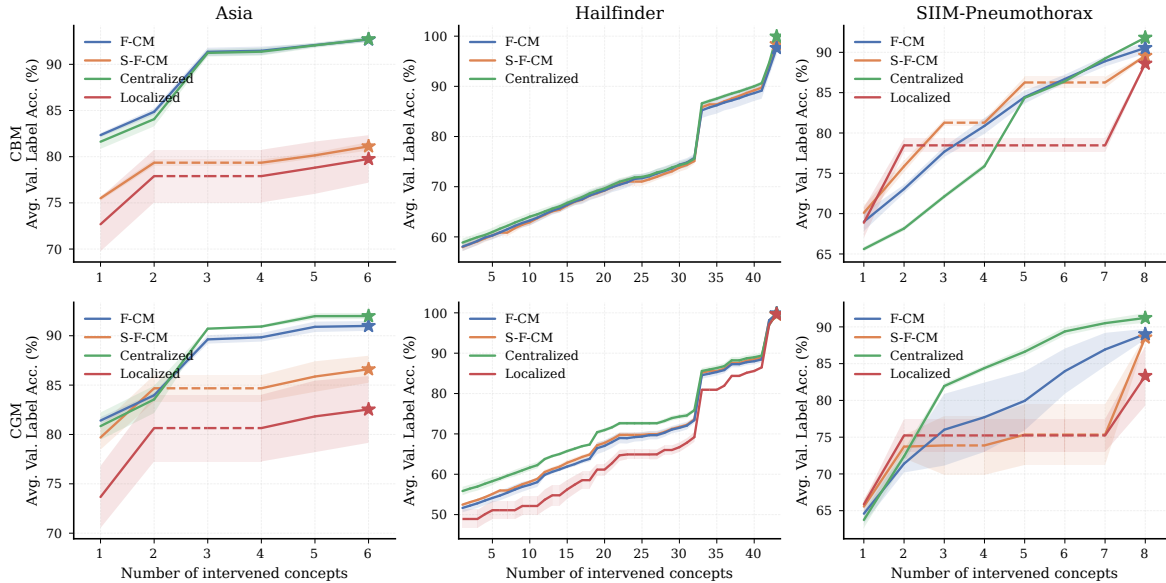


Figure 7. Label accuracy (%) on downstream variables (including the task) following interventions on concepts at increasing depths of the ground-truth graph hierarchy. Dashed lines denote interventions that are not possible for a given modality due to the absence of predictions for the corresponding concept.

Table 4. Fraction of parameters changed (%) due to *temporal non-stationarity* (dynamic participation).

Model	Asia	Sachs	Alarm	Insurance	Hailfinder	SIIM Pn.
OpaqNN	18.28 ± 5.01	38.32 ± 12.55	42.76 ± 11.40	28.90 ± 8.31	17.37 ± 5.74	5.46 ± 1.31
CBM	62.55 ± 25.35	70.00 ± 30.35	48.44 ± 15.44	26.90 ± 7.01	19.24 ± 8.25	9.27 ± 2.46
CEM	61.30 ± 23.18	81.11 ± 36.34	57.30 ± 17.33	30.44 ± 8.79	17.80 ± 6.13	21.61 ± 5.89
CGM	32.19 ± 6.22	43.09 ± 13.81	45.87 ± 19.68	19.68 ± 6.64	8.37 ± 2.85	10.29 ± 2.61
C^2BM	28.56 ± 8.89	44.82 ± 16.64	31.06 ± 9.06	19.24 ± 5.44	12.73 ± 4.01	8.49 ± 2.22

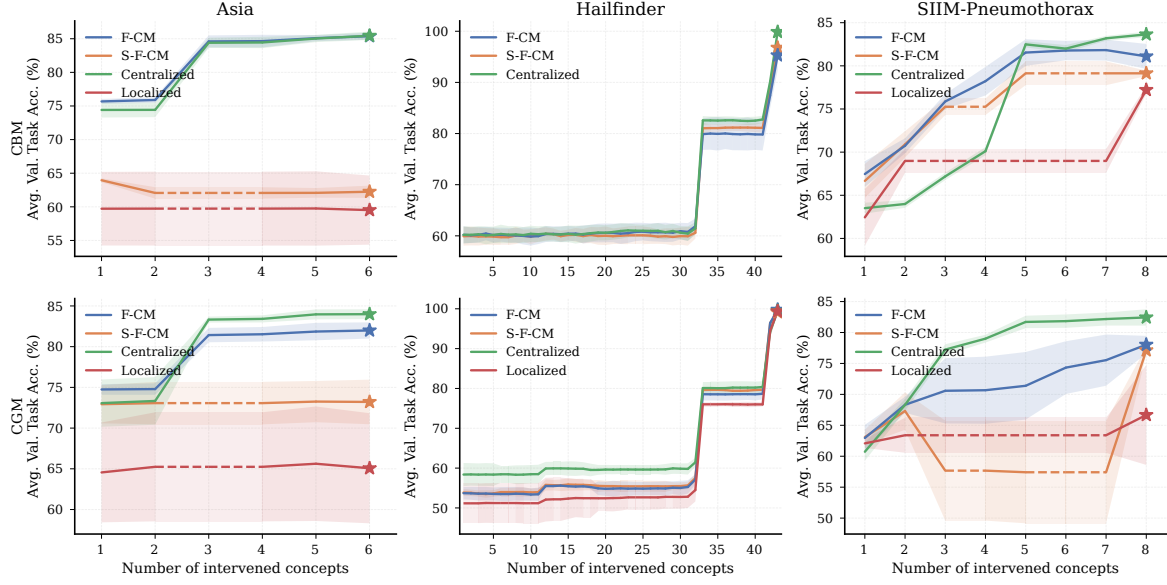


Figure 8. Task accuracy (%) following interventions on concepts at increasing depths of the ground-truth graph hierarchy. Dashed lines denote interventions that are not possible for a given modality due to the absence of predictions for the corresponding concept.

metric as a proxy for the *scope of adaptation* and *training compute-efficiency*: smaller values indicate that updates remain localized to a limited set of concept/task modules rather than inducing widespread changes.

Table 4 reports results across datasets and model instantiations. Overall, the fraction of changed parameters remains far below full retraining (i.e., $\ll 100\%$), supporting our main claim that F-CMs incorporate new supervision by updating only the affected modules while preserving the rest of the model. The magnitude of the update varies across architectures and datasets, reflecting differences in concept dimensionality and the degree to which newly introduced supervision interacts with existing modules (e.g., CEM typically changes a larger fraction than C²BM). These results complement the convergence trends in Fig. 3: sparser updates are associated with faster recovery after client arrivals, avoiding the slow restart behaviour of retraining from scratch.

E.4. Differential Privacy

To further ensure privacy in FL, we incorporate *differential privacy* (Dwork, 2006) (DP) to limit the information that can be inferred from communicated client-side statistics. DP provides a formal guarantee that the inclusion or exclusion of any single data sample has a bounded impact on the released information, thereby protecting individual participants against inference attacks. Formally, a randomized mechanism $\mathcal{M} : \mathcal{D} \rightarrow \mathcal{R}$ satisfies (ε, δ) -differential privacy if, for any pair of neighboring datasets D and D' that differ in one sample and any measurable set $\mathcal{S} \subseteq \mathcal{R}$,

$$\Pr[\mathcal{M}(D) \in \mathcal{S}] \leq e^\varepsilon \Pr[\mathcal{M}(D') \in \mathcal{S}] + \delta. \quad (3)$$

Here, ε controls the strength of the privacy guarantee, with smaller values corresponding to stronger privacy protection, while δ represents a negligible probability of privacy violation.

In practice, we enforce DP at the client update level using a standard DP-SGD pipeline implemented with Opacus (Yousefpour et al., 2022). At each local optimization step, client gradients are computed at the *per-sample* level and then *clipped* to a maximum ℓ_2 norm C :

$$g_i \leftarrow g_i \cdot \min\left(1, \frac{C}{\|g_i\|_2}\right), \quad C = 1.0. \quad (4)$$

Clipping bounds the contribution of any single sample to the update, which effectively bounds the sensitivity of the released (aggregated) gradient signal. After clipping, Gaussian noise is added to the (mini-batch) aggregated gradient before taking the optimizer step. The noise scale is chosen by the privacy accountant to meet a target privacy budget (ε, δ) given the training configuration (sampling rate, number of steps/epochs, etc.). In our experiments we fix $\delta = 10^{-5}$ and report results for $\varepsilon \in \{10, 5, 1\}$, where smaller ε corresponds to stronger privacy (and typically lower utility).

Empirical Validation. Table 5 reports task, concept, and label accuracy under DP for different privacy budgets. As expected, tightening privacy (decreasing ε) leads to a moderate degradation in performance. Notably, across most instantiations the drop from $\varepsilon = 10$ to $\varepsilon = 5$ is small, and even at $\varepsilon = 1$ several models remain competitive (e.g., OpaqNN and CEM exhibit limited degradation), indicating that F-CM-style training remains effective under strong privacy constraints. Larger drops for some architectures (e.g., CBM and CGM at $\varepsilon = 1$) are consistent with the stronger noise required at low ε and the known sensitivity of some training dynamics to DP perturbations.

Table 5. Impact of differential privacy on federated concept-based models under different privacy budgets ε . We report task accuracy and concept accuracy (mean \pm std.) for representative model instantiations.

Privacy Budget	$\varepsilon = 10$		$\varepsilon = 5$		$\varepsilon = 1$	
	Task Acc.	Concept Acc.	Task Acc.	Concept Acc.	Task Acc.	Concept Acc.
OpaqNN	80.03 \pm 0.68	90.37 \pm 0.70	79.19 \pm 0.97	89.43 \pm 1.32	77.31 \pm 0.96	89.15 \pm 1.07
C^2 BM	79.37 \pm 1.01	86.89 \pm 2.78	79.20 \pm 1.16	86.89 \pm 2.63	76.22 \pm 2.24	85.81 \pm 2.06
CBM	79.11 \pm 1.79	89.32 \pm 1.46	79.03 \pm 1.87	89.13 \pm 1.49	72.73 \pm 6.52	88.07 \pm 2.16
CEM	80.19 \pm 1.08	86.26 \pm 2.72	80.17 \pm 1.63	87.26 \pm 2.74	78.12 \pm 2.68	85.67 \pm 2.47
CGM	78.67 \pm 2.39	88.59 \pm 1.34	77.68 \pm 0.94	86.47 \pm 1.90	72.00 \pm 2.23	85.83 \pm 1.83

E.5. Sensitivity Analysis

E.5.1. NUMBER OF CLIENTS

We study the effect of scaling the number of clients by varying the total client population $K \in \{10, 20, 50, 100\}$, while keeping the overall amount of data fixed. As K increases, each client holds fewer local samples on average, resulting in smaller and more heterogeneous local datasets. This setting reflects realistic large-scale federated deployments, where data are fragmented across many participants.

Tables 6 reports task accuracy, concept accuracy, and label accuracy for different federation sizes. Across all model instantiations, performance remains stable as the number of clients increases, with only moderate degradation in accuracy for the largest federation sizes. In particular, concept accuracy exhibits limited sensitivity to increasing K , indicating that aggregating concept supervision from a larger number of smaller clients remains effective.

Architectures with richer concept representations (e.g., CEM and CBM) show the strongest robustness to client scaling, while models relying on more structured dependencies (e.g., C^2 BM and CGM) experience slightly larger variance as K grows. This behavior is consistent with the increased statistical heterogeneity and reduced local sample sizes associated with larger client populations. Overall, these results suggest that F-CMs scale gracefully with the number of clients, preserving both concept quality and downstream task performance even in highly fragmented federations.

Table 6. Scaling with the number of clients. Task accuracy and concept accuracy (mean \pm std.) as the total number of clients K increases, while keeping the overall amount of data fixed.

# Clients	$K = 10$		$K = 20$		$K = 50$		$K = 100$	
	Models	Task Acc.	Concept Acc.	Task Acc.	Concept Acc.	Task Acc.	Concept Acc.	Task Acc.
OpaqNN	80.61 \pm 1.98	91.63 \pm 0.70	79.83 \pm 0.99	90.80 \pm 0.40	80.37 \pm 1.06	90.03 \pm 0.99	79.94 \pm 1.15	90.30 \pm 0.82
C^2 BM	80.14 \pm 2.02	91.23 \pm 0.81	78.16 \pm 3.11	87.81 \pm 2.32	80.35 \pm 0.72	86.44 \pm 2.17	75.38 \pm 3.98	86.10 \pm 2.42
CBM	79.91 \pm 1.98	91.52 \pm 0.83	79.25 \pm 1.12	91.09 \pm 0.61	79.54 \pm 1.02	90.94 \pm 0.50	78.32 \pm 1.33	90.54 \pm 0.55
CEM	80.58 \pm 2.04	91.40 \pm 0.72	80.58 \pm 1.11	88.59 \pm 1.63	79.92 \pm 1.31	87.92 \pm 2.01	78.80 \pm 1.80	86.19 \pm 1.91
CGM	79.33 \pm 2.20	91.05 \pm 0.89	79.30 \pm 1.74	87.76 \pm 1.83	78.96 \pm 1.77	85.86 \pm 2.10	78.84 \pm 1.85	86.41 \pm 2.14

E.5.2. EFFECT OF SELECTIVE PARAMETER FREEZING

We evaluate the empirical impact of *selective parameter freezing*, i.e., freezing concept/task modules that lack local supervision at a client (Section 4.2.3). This mechanism enforces module-specific training by ensuring that only supervised components receive gradients, while unsupervised modules remain unchanged. Tables 7–8 show task and concept accuracy with and without freezing for two representative instantiations (C^2 BM and CEM). Overall, freezing is largely *performance-neutral*: on smaller graphs such as ASIA, the effect is minimal since only a few modules are unsupervised at each client.

Table 7. Effect of selective parameter freezing (Asia/Sachs/Alarm). Task and concept accuracy (mean \pm std.) across 5 seeds, comparing standard training (No) vs. selective freezing of unsupervised modules (Yes).

Model	Freezing	Asia		Sachs		Alarm	
		Task Acc.	Concept Acc.	Task Acc.	Concept Acc.	Task Acc.	Concept Acc.
C ² BM	No	80.35 \pm 2.16	90.55 \pm 0.95	76.20 \pm 2.08	72.22 \pm 1.68	73.14 \pm 0.78	90.23 \pm 0.30
	Yes	80.52 \pm 1.00	90.47 \pm 0.58	76.55 \pm 0.98	72.73 \pm 0.71	72.60 \pm 0.57	89.12 \pm 0.38
CEM	No	80.50 \pm 1.66	89.77 \pm 2.04	75.97 \pm 2.56	73.03 \pm 1.36	73.42 \pm 0.44	90.10 \pm 0.55
	Yes	80.27 \pm 0.89	90.07 \pm 0.86	76.43 \pm 1.16	73.33 \pm 0.63	72.70 \pm 0.22	89.80 \pm 0.32

Table 8. Effect of selective parameter freezing (Insurance/Hailfinder/SIIM). Task and concept accuracy (mean \pm std.) across 5 seeds, comparing standard training (No) vs. selective freezing of unsupervised modules (Yes).

Model	Freezing	Insurance		Hailfinder		SIIM Pn.	
		Task Acc.	Concept Acc.	Task Acc.	Concept Acc.	Task Acc.	Concept Acc.
C ² BM	No	74.27 \pm 2.34	76.08 \pm 1.20	72.83 \pm 2.06	57.66 \pm 1.41	68.80 \pm 2.51	67.68 \pm 1.32
	Yes	74.10 \pm 1.35	76.00 \pm 0.62	71.70 \pm 0.81	56.46 \pm 0.62	65.90 \pm 1.34	64.91 \pm 1.37
CEM	No	70.97 \pm 0.75	77.16 \pm 0.70	70.15 \pm 3.82	60.13 \pm 1.25	67.33 \pm 2.68	64.90 \pm 1.57
	Yes	71.30 \pm 1.01	76.82 \pm 0.62	70.20 \pm 1.89	59.30 \pm 0.68	66.91 \pm 1.30	65.88 \pm 1.45

However, on larger benchmarks (e.g., ALARM, HAILFINDER, SIIM), where the model contains more concept modules and parent-conditioned dependencies, freezing can slightly improve stability by preventing updates to poorly-supported components and reducing update noise. Beyond accuracy, freezing provides a practical efficiency benefit at the client side, as it reduces the number of trainable parameters during local optimization (lower gradient/optimizer-state footprint and compute), while remaining fully consistent with our module-wise aggregation protocol.

E.6. Robustness to graph perturbations

In this section, we evaluate the sensitivity of the DAG aggregation procedure (Section 4.2.1) to noise in client-provided graphs, which can arise both from limited local data (estimation error) and from adversarial behavior (e.g., poisoning the communicated structure) (Sun et al., 2022; Fenoglio et al., 2024). To reduce variance due to a specific client partition, we run this experiment with a large federation and high per-round participation. Concretely, training follows the same temporal non-stationarity setup as in the main paper, but with $|\mathcal{K}_t| = 100$ participating clients per round. The client pool is time-varying: during a warm-up phase the federation contains $|\mathcal{K}(t)| = 100$ clients, and at the predefined join round (as in our standard protocol, depending on the dataset) an additional cohort joins, expanding the pool to $|\mathcal{K}(t)| = 200$. Late-arriving clients may introduce new concepts and associated edges, requiring the aggregated shared structure to expand accordingly.

Each participating client provides a local graph (binary adjacency matrix) over its observed variables. We inject noise by randomly deleting, adding, or reversing edges, while enforcing acyclicity. We vary two factors: (*% client alteration*), the fraction of clients whose graphs are corrupted, and (*graph alteration*), the fraction of edges modified within each corrupted client graph. Aggregation quality is measured by *DiffPairs*, i.e., the number of node pairs whose relative ordering differs between the aggregated shared DAG and the reference DAG (lower is better). Figure 9 reports results for the federated regimes (F-CMs and S-F-CMs) and includes localized training (Loc.) as a reference.

Empirical Validation. Overall, the proposed server-side graph aggregation is robust to substantial client-side noise. In particular, for moderate perturbations (e.g., 30% graph alteration), the aggregated structure remains essentially unchanged across the full range of % client alteration: *DiffPairs* stays nearly constant for both F-CMs and S-F-CMs. This indicates that the aggregation effectively denoises inconsistent local proposals when the per-client corruption level is limited. In contrast, the Localized baseline exhibits a markedly different behavior: for a fixed graph alteration level, *DiffPairs* increases approximately linearly with % client alteration, reflecting the lack of cross-client averaging and the direct propagation of local graph errors to the deployed structure.

At higher corruption levels, *DiffPairs* increases as expected. For 60% graph alteration, degradation becomes visible once a large majority of clients are corrupted (typically around 60–70% corrupted clients across datasets). For 90% graph alteration,

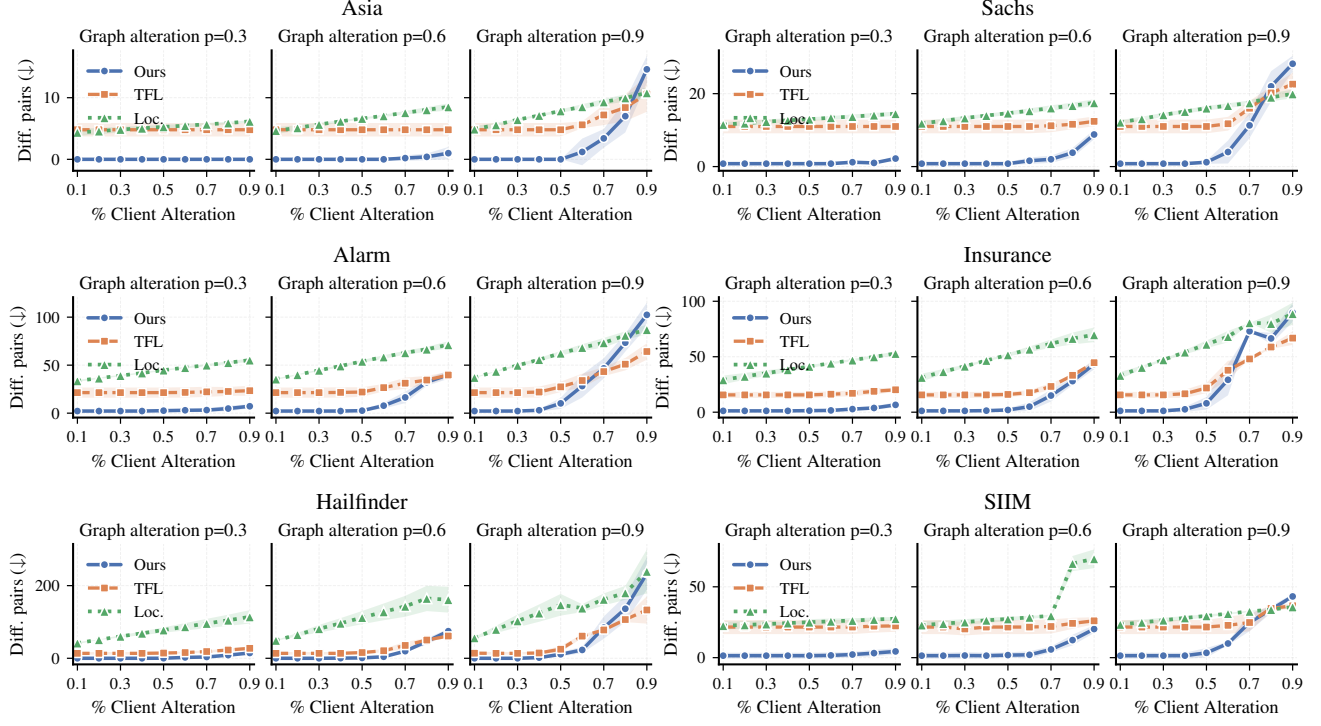


Figure 9. **Robustness of DAG aggregation to client graph perturbations.** DiffPairs (lower is better) between the aggregated DAG and the ground-truth DAG as a function of %client alteration and per-client graph alteration.

the effect appears earlier, becoming pronounced already around 50% corrupted clients. Finally, the gap between F-CMs and S-F-CMs is primarily explained by *structure evolution*: S-F-CMs does not update the shared graph when late-arriving clients introduce new concepts and edges, leading to an increasingly partial global view, whereas F-CMs continuously integrates new proposals and maintains coverage of the evolving federation.